



Effect of surface functionalization of halloysite nanotubes on synthesis and thermal properties of poly(ϵ -caprolactone)

Zoi Terzopoulou¹ , Dimitrios G. Papageorgiou², George Z. Papageorgiou³, and Dimitrios N. Bikiaris^{1,*} 

¹Laboratory of Polymer Chemistry and Technology, Department of Chemistry, Aristotle University of Thessaloniki, 54124 Thessaloniki, Greece

²School of Materials and National Graphene Institute, University of Manchester, Oxford Road, Manchester M13 9PL, UK

³Department of Chemistry, University of Ioannina, P.O. Box 1186, 45110 Ioannina, Greece

Received: 10 November 2017

Accepted: 3 January 2018

Published online:
16 January 2018

© Springer Science+Business
Media, LLC, part of Springer
Nature 2018

ABSTRACT

In this work, halloysite nanotubes (HNTs) and functionalized HNTs–APTES (aminopropyltriethoxysilane) in concentrations 0.5, 1 and 2.5 wt% were used as nanofillers in the synthesis of poly(ϵ -caprolactone) (PCL) nanocomposites via the in situ ring-opening polymerization of ϵ -caprolactone (CL). The successful functionalization of HNTs was confirmed with X-ray photoelectron spectroscopy. The effects of HNTs and HNTs–APTES on the polymerization procedure and on the thermal properties of PCL were studied in detail. It was found that both nanofillers reduced the \bar{M}_n values of the resulting nanocomposites, with the unfunctionalized one reducing it in a higher extent, while SEM micrographs indicated satisfactory dispersion in the PCL matrix. The crystallization study under isothermal and dynamic conditions revealed the nucleating effect of the nanotubes. The functionalization of nanotubes enabled even faster rates and attributed higher nucleation activity as a result of better dispersion and the formation of a strong interface between the filler and the matrix. An in-depth kinetic analysis was performed based on the data from crystallization procedures. PLOM images confirmed the effectiveness of both fillers as heterogeneous nucleation agents. Finally, from TGA analysis, it was found that HNTs did not affect the thermal stability of PCL while for HNTs–APTES, a small decrease in T_{\max} was observed, of about 5 °C for all filler contents.

Address correspondence to E-mail: dbic@chem.auth.gr

Introduction

Polymer nanocomposites are a class of materials consisting of a polymeric matrix containing organic or inorganic nanofillers, and it is a steadily growing field both among academia as well as industry [1], owing the unique, versatile effect that nanofillers can have on polymeric materials. Some of the properties of polymers that can be altered based on the target application by the incorporation of nanofillers are mechanical [2], thermal [3, 4], crystallization [5–9], electrical [10], magnetic [11], optical [12] and biological properties [13]. Nanoclays are one important category of nanofillers that has been extensively studied during the last decades, including layered silicates and nanosized clay minerals. They possess important advantages such as low cost, abundance, relatively large aspect ratios and can be easily chemically or physically functionalized; as a result, they are already being used in the paper and ceramics industries, as well as in oil drilling [14, 15]. However, their layered structure makes exfoliation into individual sheets challenging, since strong interlayer bonds exist between the layers, forming agglomerated tactoids in nanocomposites.

Halloysite is a different type of clay nanofiller, since in contrast with the common layered aluminosilicate minerals, it possesses a nanotubular structure with high aspect ratio. Its chemical composition is similar to that of kaolinite ($\text{Al}_2\text{Si}_2\text{O}_5(\text{OH})_4 \cdot n\text{H}_2\text{O}$) [16]. Owing its structure, it shows a variety of unique properties that make it attractive for applications in polymeric nanocomposites, drug release and biomedical applications [17, 18]. The inner surface of the nanotubes is comprised of aluminol groups, and the outer mainly of siloxanes, with a few aluminols and silanols on the defects of the outer edges [1]. That makes HNTs relatively hydrophobic, which makes their dispersion in non-polar polymers easy, while the few hydroxyls on the surface provide with active sites for chemical functionalization [18]. The nanotubular structure also makes HNTs a great carrier for biologically active substances [17].

PCL is an aliphatic, biodegradable polyester that can be synthesized either by the ring-opening polymerization of ϵ -CL, or by the polycondensation of 6-hydroxyhexanoic acid. It is a semi-crystalline, hydrophobic polymer with low melting temperature (59–64 °C). PCL is a FDA-approved polymer [19] for

hard and soft tissue applications, biocompatible and miscible with several polymers, easily processed and molded, properties that led to a wide range of applications, especially in tissue engineering, drug delivery and food packaging [20, 21]. Nevertheless, its poor thermal and mechanical properties prevent PCL from being used in load bearing applications; however they can be tailored with the use of nanofillers [4].

Polymeric nanocomposites containing HNTs can be synthesized with the already established methods for nanocomposite fabrication, i.e., solution casting, melt mixing and in situ polymerization [22]. In situ polymerization possesses several advantages as a technique for the fabrication of nanocomposites, such as one-pot synthesis of nanocomposites, better dispersion of the fillers compared with the other methods, improved interfacial adhesion, and consequently better properties of the final product [22–26]. Despite its superiority, in situ polymerization has not been studied in a great extend for the preparation of nanocomposites of polyesters with HNTs. Lahcini et al. synthesized PCL/HNTs nanocomposites via the ring-opening polymerization of ϵ -CL and found that the hydroxyl groups of HNTs can act as co-initiators along with tin tetrachloride [27]. Other in situ synthesized nanocomposites reinforced with HNTs that exhibited enhanced properties were based on polyethylene/ethylene methacrylate copolymer [28], polypropylene [29], polystyrene [30, 31], poly(vinyl chloride) [32], and biobased polyurethanes [33, 34].

In order to improve the interfacial adhesion of HNTs with polymeric matrices, several methods for their surface functionalization have been employed [1]. One of the most common ones is organosilylation, with several silanes containing different end groups [19]. Grafting of 3-aminopropyltriethoxysilane (APTES) on the surface of HNTs was found to improve their dispersion in PLA:PCL nanofibers [35] and in polypropylene nanocomposites prepared by injection molding [36]. Vinyltrimethoxysilane functionalization improved interfacial adhesion in unsaturated polyester nanocomposites with HNTs [37], while tetraethoxysilane grafting improved the barrier properties and decreased moisture absorption of polyimide/HNTs nanocomposites [38]. In the present study, γ -aminopropyltriethoxysilane (APTES) was used to functionalize HNTs because its amino group can interact with the ϵ -CL monomer during ring-

opening polymerization and form covalent bonds, resulting in strong bonding between HNTs and PCL, which is expected to improve the dispersion and properties of the final nanocomposite materials [39].

The aim of this study is the synthesis of PCL nanocomposites with HNTs and HNTs–APTES with in situ ring-opening polymerization of ϵ -CL. The effect of the functionalization and content of HNTs on the thermal and crystallization properties of PCL were studied with a number of experimental techniques, including intrinsic viscosity measurements, scanning electron microscopy (SEM), wide-angle X-ray diffraction (WAXD), differential scanning calorimetry (DSC), polarizing light optical microscopy (PLOM) and thermogravimetric analysis (TGA).

Experimental

Materials

Halloysite nanoclay (kaolin clay) has the molecular formula $\text{Al}_2\text{Si}_2\text{O}_5(\text{OH})_4 \cdot 2\text{H}_2\text{O}$ and molecular weight 249.19 amu. Its surface area was measured equal to $53.3 \text{ m}^2/\text{g}$ with 0.371 mL/g pore volume and the approximate size of nanotubes was $30\text{--}70 \text{ nm} \times 3\text{--}8 \text{ }\mu\text{m}$. ϵ -Caprolactone (CL) monomer was of purity 99% and was further purified by distillation. Catalyst tetrabutyl titanate (TBT) and γ -aminopropyltriethoxysilane (APTES) were of analytical grade. All chemicals were supplied by Sigma-Aldrich.

Functionalization of nanofillers

HNTs were dehydrated at $100 \text{ }^\circ\text{C}$ under vacuum and functionalized with APTES in order to add amine reactive groups on their surface. Briefly, 2 g of APTES was dissolved in dry toluene, and 2 g of nanoclay was dispersed in the reaction mixture with the help of ultrasonic treatment. The reaction was refluxed at $120 \text{ }^\circ\text{C}$ for 20 h, while a calcium chloride tube was attached to the system. The solid phase was filtered and washed 3 times with toluene and 3 times with ethanol to ensure the removal of excess organosilane [40].

Synthesis of nanocomposites

For the synthesis of PCL, ϵ -CL was dried over CaH_2 and purified by distillation under reduced pressure

prior to use. The bulk polymerization of ϵ -CL was carried out in 250-mL round-bottom flask equipped with a mechanical stirrer and a vacuum apparatus. The catalyst TBT was added as a solution in toluene at a final concentration of $1 \times 10^{-4} \text{ mol per mole of monomer}$. The polymerization mixture was de-gassed and purged with dry argon three times. The ring-opening polymerization (ROP) reaction was carried out for 2 h at $190 \text{ }^\circ\text{C}$, followed by increasing of the reaction temperature from 210 to $240 \text{ }^\circ\text{C}$ over a period of 45 min. Unreacted monomer was removed through distillation by applying a high vacuum ($\approx 5 \text{ Pa}$) slowly, to avoid excessive foaming, over a time period of 15 min. Polymerization was terminated by rapid cooling to room temperature.

For the preparation of PCL/HNTs and PCL/HNTs–APTES nanocomposites by in situ polymerization the same procedure was followed. HNTs or HNTs–APTES together with the proper amount of TBT were added in ϵ -CL monomer and were sonicated initially for 2 min using a tip sonication apparatus, and then in a sonic bath for 15 min. Polymerization was then carried out. Nanocomposites containing 0.5, 1 and 2.5 wt% HNTs and HNTs–APTES have been prepared.

The prepared materials were afterward hot pressed using an Otto Weber, Type PW 30 hydraulic press connected with an Omron E5AX Temperature Controller, at a temperature of $75 \pm 5 \text{ }^\circ\text{C}$, in order to prepare films of different thicknesses, appropriate for each type of following measurements.

Characterization techniques

TEM experiments were carried out on a JEOL 2011 TEM with a LaB6 filament and an accelerating voltage of 200 kV. The specimens were prepared by evaporating drops of HNT and HNT–APTES ethanol suspensions after sonication onto a carbon-coated lacy film supported on a 3 mm diameter, 300 mesh copper grid.

The element composition and interfacial interactions were studied using X-ray photoelectron spectroscopy (XPS). In the XPS analysis (AXIS Ultra 'DL' X-ray photoelectron spectrometer) (Shimadzu Corp., Japan), a monochromatic Al K α X-ray was used at 14 kV. A binding energy of 284.8 eV for the C 1s of aliphatic carbons was taken as the reference energy. XPS curve fitting of was accomplished using Kratos' Vision 2 Processing software.

Fourier transform infrared spectroscopy (FTIR) spectra of all the samples were obtained using a Perkin-Elmer FTIR spectrometer, model Spectrum One. The materials were in the form of thin films with thickness of approximately 15 μm . The IR spectra of these films were obtained in absorbance mode and in the spectral region of 400–4,000 cm^{-1} using a resolution of 4 cm^{-1} and 64 co-added scans.

Wide-angle X-ray diffraction (WAXD) measurements of the samples were performed using a Mini-Flex II XRD system from Rigaku Co, with $\text{CuK}\alpha$ radiation ($\lambda = 0.154 \text{ nm}$) at the area of $5 < 2\theta < 60^\circ$. Crystallinity calculations of the studied materials were performed by fitting the WAXD profiles with Gaussian–Lorentzian cross product curves and deriving the ratio of crystalline over overall fitted peaks area [41, 42]. Crystallinity of the polyesters was determined by Eq. 1:

$$\% \text{Crystallinity} = \frac{\text{Area under crystalline peaks}}{\text{Total area under peaks}} \cdot 100\% \quad (1)$$

Nitrogen adsorption/desorption experiments at -196°C were performed for the determination of surface area (multi-point BET method), total pore volume (at $P/P_0 = 0.99$), and pore size distribution (BJH method using adsorption data) of the HNT and HNT–APTES samples which were previously out-gassed at 250 and 80 $^\circ\text{C}$, respectively, for 16 h under 6.6×10^{-9} mbar vacuum using an Automatic Volumetric Sorption Analyzer (Autosorb-1MP, Quantachrome).

Intrinsic viscosity $[\eta]$ measurements were performed using an Ubbelohde viscometer at 30 $^\circ\text{C}$ in toluene. The sample was maintained in the solvent at room temperature for some time in order to achieve a complete solution. The solution was then filtered through a disposable membrane filter made from Teflon. Intrinsic viscosity of the samples was calculated using the Solomon–Ciuta equation:

$$[\eta] = \frac{\sqrt{2 \cdot \left(\frac{t}{t_0} - \ln \frac{t}{t_0} - 1 \right)}}{C} \quad (2)$$

where C the concentration of the solution, t the flow time and t_0 the flow time of the solvent. The number-average molecular weight (\bar{M}_n) of the samples was calculated from the intrinsic viscosity values using the following equation [43]:

$$[\eta] = 1.4 \cdot 10^{-4} \cdot \bar{M}_n^{0.78} \quad (3)$$

The morphology of the prepared nanocomposites was examined using a scanning electron microscopy system (SEM) type JEOL (JMS-840) (Jeol Ltd., Tokyo) equipped with an energy-dispersive X-ray (EDX) Oxford ISIS 300 micro-analytical system (Oxford Instruments UK). The studied surfaces were coated with carbon black in order to obtain good conductivity for the electron beam. Operating conditions were: accelerating voltage 20 kV, probe current 45 nA and counting time 60 s.

All differential scanning calorimetry experiments were performed on a TA Instruments TMDSC (TA Q2000) combined with a cooling accessory and calibrated with indium for the heat flow and temperature measurements. All sample masses were kept close to 5 mg and the Tzero sample and reference pans were of identical mass. The samples were initially heated to 50 $^\circ\text{C}$ higher than the melting point and held there for 5 min in order to erase any thermal history. Afterward, the sample was quenched to -90°C and then reheated with 10 $^\circ\text{C min}^{-1}$. The glass transition temperature and the melting points were recorded this way. For non-isothermal crystallization, the samples were heated from room temperature up to 140 $^\circ\text{C}$, held there for 5 min and cooled down to room temperatures at rates varying from 5 to 20 $^\circ\text{C min}^{-1}$. A fresh sample was used in each run.

For the isothermal crystallization experiments, temperatures of 40–46 $^\circ\text{C}$ were pre-selected and the experiments were performed after self-nucleation of the polyester samples, in a procedure proportional with the one described by Muller et al. [44–46]. The protocol can be summarized as follows: (a) heating of the sample and remaining at 140 $^\circ\text{C}$ or at the proper temperature for each copolymer for 5 min in order to erase any previous thermal history; (b) subsequent cooling at a rate of 10 $^\circ\text{C min}^{-1}$ –40 $^\circ\text{C}$ or at the proper temperature for each copolymer and crystallization for 10 min, which creates a “standard” thermal history; (c) partial melting by heating at 20 $^\circ\text{C min}^{-1}$ up to a “self-nucleation temperature,” T_s ; thermal conditioning at T_s for 1 min. Depending on T_s , the crystalline polyester domains will be completely molten, only self-nucleated or self-nucleated and annealed. If T_s is sufficiently high no self-nuclei or crystal fragments can remain and the sample is then in the so-called Domain I, the

complete melting domain. At intermediate T_s values, the sample is almost completely molten but some small crystal fragments or crystal memory effects remain, which can act as self-nuclei during a subsequent cooling from T_s , and the sample is said to be in Domain II, the self-nucleation domain. Finally, if T_s is too low, the crystals will only be partially molten, and the remaining crystals will undergo annealing during the 5 min at T_s , while the molten crystals will be self-nucleated during the later cooling, and the sample is in Domain III, the self-nucleation and annealing domain.; (d) cooling scan from T_s at $200\text{ }^\circ\text{C min}^{-1}$ to the crystallization temperature (T_c), where the effects of the previous thermal treatment will be reflected on crystallization; (e) heating scan at $20\text{ }^\circ\text{C min}^{-1}$ to $120\text{ }^\circ\text{C}$ or to the proper temperature for each copolymer, where the effects of the thermal history will be apparent on the melting signal. Experiments were performed to check that the sample did not crystallize during the cooling to T_c and that a full crystallization exothermic peak was recorded at T_c . In heating scans after isothermal crystallization, the standard heating rate was $20\text{ }^\circ\text{C min}^{-1}$. If some other rate was used, this will be discussed in the specific section.

A polarizing light microscope (Nikon, Optiphot-2) equipped with a Linkam THMS 600 heating stage, a Linkam TP 91 control unit and a Jenoptic ProgRes C10Plus camera was used for PLM observations.

Thermogravimetric analysis was carried out with a Setsys 16/18 TG-DTA (Setaram). Samples ($4 \pm 0.2\text{ mg}$) were placed in alumina crucibles and heated from ambient temperature to $620\text{ }^\circ\text{C}$ at $20\text{ }^\circ\text{C min}^{-1}$ in a 50 ml min^{-1} flow of N_2 ; an empty alumina crucible was used as reference.

Results and discussion

Functionalization of HNTs

Initially, the morphology of HNTs was studied by TEM images (Fig. 1). The HNTs clearly possess a tubular structure with multilayer walls, and their lumen is open to the ends of each tube. The lumen's diameter was calculated between 9 and 12 nm and the outer diameter 30–70 nm. Their length appears to vary, ranging from 3 to 8 μm . The tubular morphology is retained after the functionalization reaction (Fig. 1b); however, the diameter of HNTs appears to

be slightly bigger, up to 110 nm. This can be attributed to the possible formation of a thin layer or oligomerized APTES on the surface of HNTs that could lead to increased external diameter [40].

Silylation is one of the most common methods to covalently functionalize HNTs, and the reaction occurs between the hydroxyl groups on the surface of the nanotubes and the silanol groups of the silane. It has been found that besides the direct bonding of APTES on the hydroxyls, oligomerization of hydrolyzed silane can also take place in the presence of physically absorbed water [47]. FTIR spectra of pure and functionalized HNTs are presented in Fig. S1. The characteristic peaks observed can be attributed to hydroxyls ($3600\text{--}3700\text{ cm}^{-1}$), planar Si–O stretching ($1025\text{--}1050\text{ cm}^{-1}$), symmetric Si–O bending (795 cm^{-1}), vertical Si–O bending ($690, 795\text{ cm}^{-1}$) and Al–O–Si stretching (475 cm^{-1}). After the functionalization procedure, a few extra peaks appear on the spectrum that are caused by the N–H₂ bending ($1560, 1490\text{ cm}^{-1}$) and symmetric C–H stretching (2936 cm^{-1}) of APTES.

The surface atomic percentages as determined by XPS are summarized in Table 1, and the high-resolution XPS spectra of HNTs and HNTs–APTES are presented in Fig. S2 and S3, respectively. HNTs contain oxygen, silicon and aluminum with a Si/Al ratio of 1, typical for a two layered aluminosilicate. The small amount of carbon detected is due to surface organic contamination. The success of the organosilane grafting is confirmed by the increase in Si and C atomic percentages, the emerging of peaks that correspond to nitrogen, and the increase in the Si/Al ratio [19]. The N 1s band (Fig. S3e) can be deconvoluted into 2 peaks at 407 and 405 eV that correspond to protonated amino groups and N–H bonds of free amino groups, respectively, [48]. The reaction that took place between HNTs and APTES is presented in Scheme 1.

X-ray diffraction patterns of pure and functionalized HNTs are presented in Fig. S4. The characteristic peak of the (001) crystal plane of HNTs appears at 11.56° with a lattice spacing of $d = 7.68\text{ \AA}$ (determined by Bragg's law) that shifts to 11.18° with $d = 7.94\text{ \AA}$ after functionalization. This indicates the HNT is type halloysite-7 \AA , i.e., the dehydrated form [18, 47, 49]. Moreover, HNTs exhibit diffraction peaks at $2\theta = 19.7^\circ$ and 24.16° that result from the crystal planes (110) and (002), respectively, and shift to $2\theta = 19.16^\circ$ and 23.78° [50]. The organosilylation of

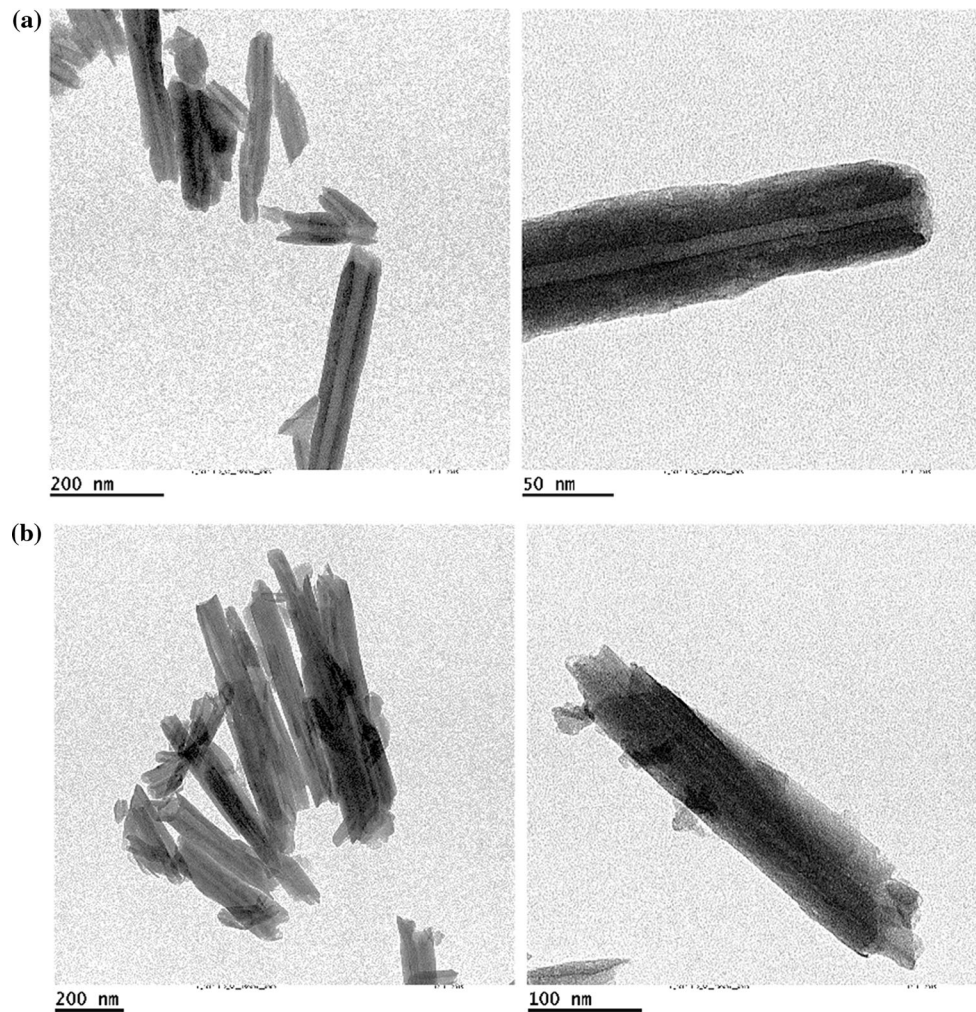


Figure 1 TEM images of **a** HNTs, **b** HNTs-APTES.

Table 1 Surface atomic percentages determined by XPS for HNTs and HNTs-APTES

Material	Surface atomic %					
	C 1s	O 1s	Si 2p	Al 2p	N 1s	Si/Al
HNTs	9.22	65.59	12.74	12.45	–	1
HNTs-APTES	25.52	46.80	13.27	8.20	6.21	1.6

HNTs did not affect the crystalline structure; however, it led to increase in the basal spacing of HNTs.

The effect of the organosilylation on the surface area and pore volume of HNTs was studied by nitrogen adsorption/desorption experiments with the multi-point BET method. The nitrogen adsorption–desorption isotherms and the respective pore size distribution curves of HNTs and HNTs-APTES

are shown in Figs. S5 and S6, respectively, while the surface area, total pore volume, and average pore size data are presented in Table 2. HNTs have a surface area value of $53.5 \text{ m}^2/\text{g}$, which is reduced to $47.2 \text{ m}^2/\text{g}$ after functionalization. This can be attributed to the presence of silane molecules and the changes in the stacking of the nanotubes [19]. The isotherm curves of Fig. S5 are characterized as type IIb which is typical for natural clays, possessing very small hysteresis loops that reveal the presence of large mesopores [47].

TGA thermograms of HNTs and HNTs-APTES are presented in Fig. S7. The first step of weight loss occurs at 87 and 104 °C for HNTs and HNTs-APTES, respectively, and is caused by loss of free interlayer water, about 3% in both cases [51]. Pure HNTs lose 14.3% of their weight between 400 and 500 °C that can be attributed to the decarboxylation of the

Scheme 1 Schematic presentation of the functionalization reaction of HNTs with APTES.

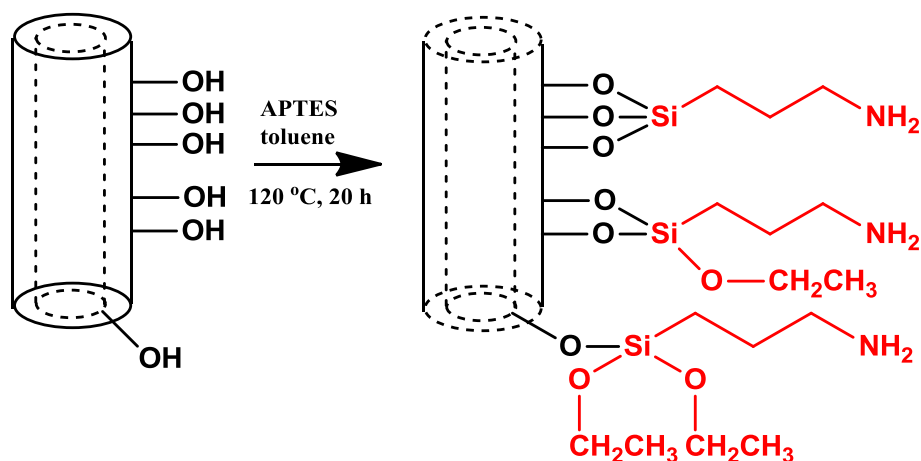


Table 2 Porosity characteristics of HNTs and HNTs–APTES

Sample	Surface area (m ² /g)	Total pore volume (mL/g)
HNTs	53.3	0.371
HNTs–APTES	47.2	0.428

Table 3 Molecular weights determined by viscometry

Sample	$[\eta]$ (dL/g)	\bar{M}_n
PCL	0.78	63435
PCL HNTs 0.5%	0.74	59295
PCL HNTs 1.0%	0.68	53204
PCL HNTs 2.5%	0.54	39591
PCL HNTs–APTES 0.5%	0.76	61357
PCL HNTs–APTES 1.0%	0.72	57249
PCL HNTs–APTES 2.5%	0.69	54209

aluminol groups that are present on the surface of the nanotubes [18, 19]. HNTs–APTES lose 16.5% of their weight in the same temperature region and that 2.2% of extra weight loss can be attributed to the degradation of the organosilane. The organic content of HNTs–APTES clearly reduces their thermal stability, as expected.

Synthesis and characterization of PCL nanocomposites

Synthesis of PCL nanocomposites via *in situ* polymerization

The ROP of CL is effectively catalyzed by metal alkoxides, such as TBT, with the first step of the reaction mechanism being the complexation with the

monomer at the carboxyl oxygen, followed by the insertion of the lactone into the metal–oxygen bond [52]. Molecular weight values, as determined by IV measurements, are presented in Table 3. The presence of the nanofillers in the polymerization mixture resulted in lower molecular weight compared to neat PCL, which has a \bar{M}_n value of 63435, while all nanocomposites display lower \bar{M}_n , ranging from 39591 to 61357. The effect of the nanofillers on the \bar{M}_n is more pronounced as the nanotube concentration in the polymeric matrix increases. The hydroxyl groups of HNTs and the amino groups of HNTs–APTES could act as co-initiators for the ROP of CL that would lead to a higher concentration of chain-ends and therefore lower molecular weight values [27, 39]. In the case of HNTs–APTES, higher \bar{M}_n values were obtained in comparison with unfunctionalized HNTs. This could be attributed to the fact that every 3 of their surface hydroxyls were used as binding sites for the organosilane, making the number of the –NH₂ groups smaller than the number of free hydroxyls in unfunctionalized HNTs. It has also been suggested by Vassiliou et al. [43] that this reduction in the \bar{M}_n could be caused by the trapping of the active catalyst species in heterogeneous exchange reaction between the TBT and the nanofiller's surface silanol groups. However, all synthesized polymers exhibited satisfactory IV and \bar{M}_n values that rendered them suitable for further characterization and confirmed the synthesis parameters as viable.

Morphological characterization

Morphological observation of the nanocomposites was conducted by SEM (Figs. 2, 3). The dispersion of

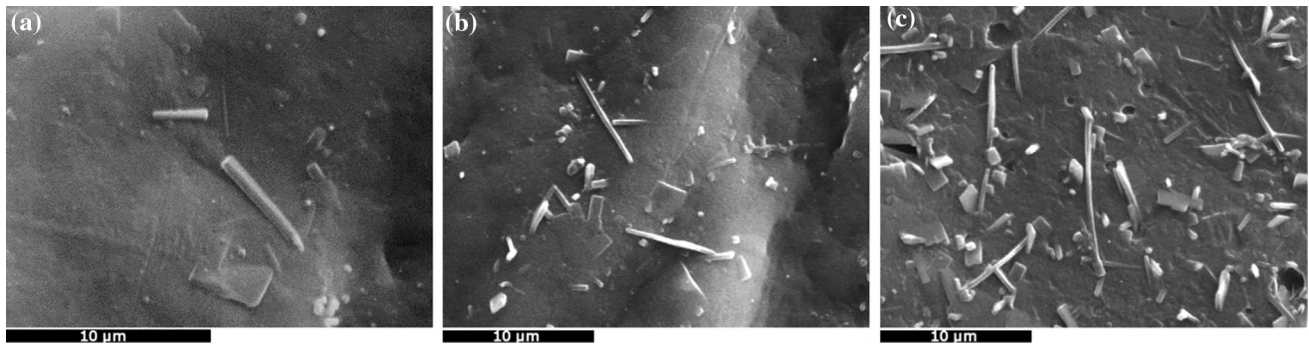


Figure 2 SEM micrographs of **a** PCL/HNTs 0.5%, **b** PCL/HNTs 1.0%, **c** PCL/HNTs 2.5 wt% in different magnifications.

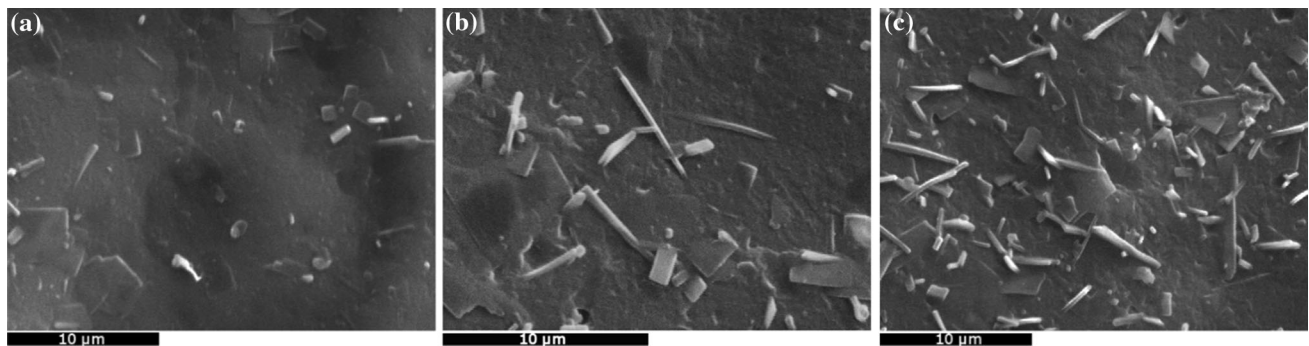


Figure 3 SEM micrographs of **a** PCL/HNTs APTES 0.5%, **b** PCL/HNTs APTES 1.0%, **c** PCL/HNTs APTES 2.5 wt% in different magnifications.

nanofillers is one of the most important factors that affect the final performance and properties of nanocomposites, since aggregates can act as premature failure points and result in low mechanical properties. HNTs appear to be well dispersed in the polymeric matrix, with no obvious aggregates, in all HNT contents. However, a number of individual nanotubes are sticking out of the surface and appear to be not fully embedded into the PCL matrix. Functionalization of inorganic nanofillers with organic compounds enhances their chemical affinity with polymeric matrices, resulting in stronger interactions, homogenous dispersion and improved mechanical properties [53]. Compared to unfunctionalized nanotubes, HNTs–APTES (Fig. 3) appears to be better entrapped into PCL, especially in the lowest concentrations 0.5, since less nanotubes are sticking out of the surface, suggesting the formation of a stronger interface between the components of the system. In both cases, dispersion appeared to be satisfactory, with no visible aggregates.

Structural characterization

FTIR spectra of PCL and the nanocomposites are presented in Fig. 4a, b. The characteristic peaks of PCL can be observed with no noticeable differences in the presence of the nanofillers. The strongest bands correspond to asymmetric CH_2 stretching at 2942 cm^{-1} , symmetric CH_2 stretching at 2865 cm^{-1} , carbonyl stretching at 1728 cm^{-1} , asymmetric COC stretching at 1243 cm^{-1} , and symmetric COC stretching at 1173 cm^{-1} . Due to the small HNT content, filler peaks cannot be detected in the spectra. However, alterations on the peak intensities and ratios before and after HNT incorporation were noticed. Therefore, carbonyl indices of PCL and its nanocomposites were calculated by dividing the integral normalized intensity of the $\text{C}=\text{O}$ peak at 1728 cm^{-1} with the sum of the normalized integral intensities of the $-\text{CH}_2-$ peaks at 1470 and 1398 cm^{-1} , and the results are presented in Fig. 4c. The number of carbonyls increased with increasing HNT content, with a more pronounced increase for the nanocomposites with HNT–APTES. This increase could be due

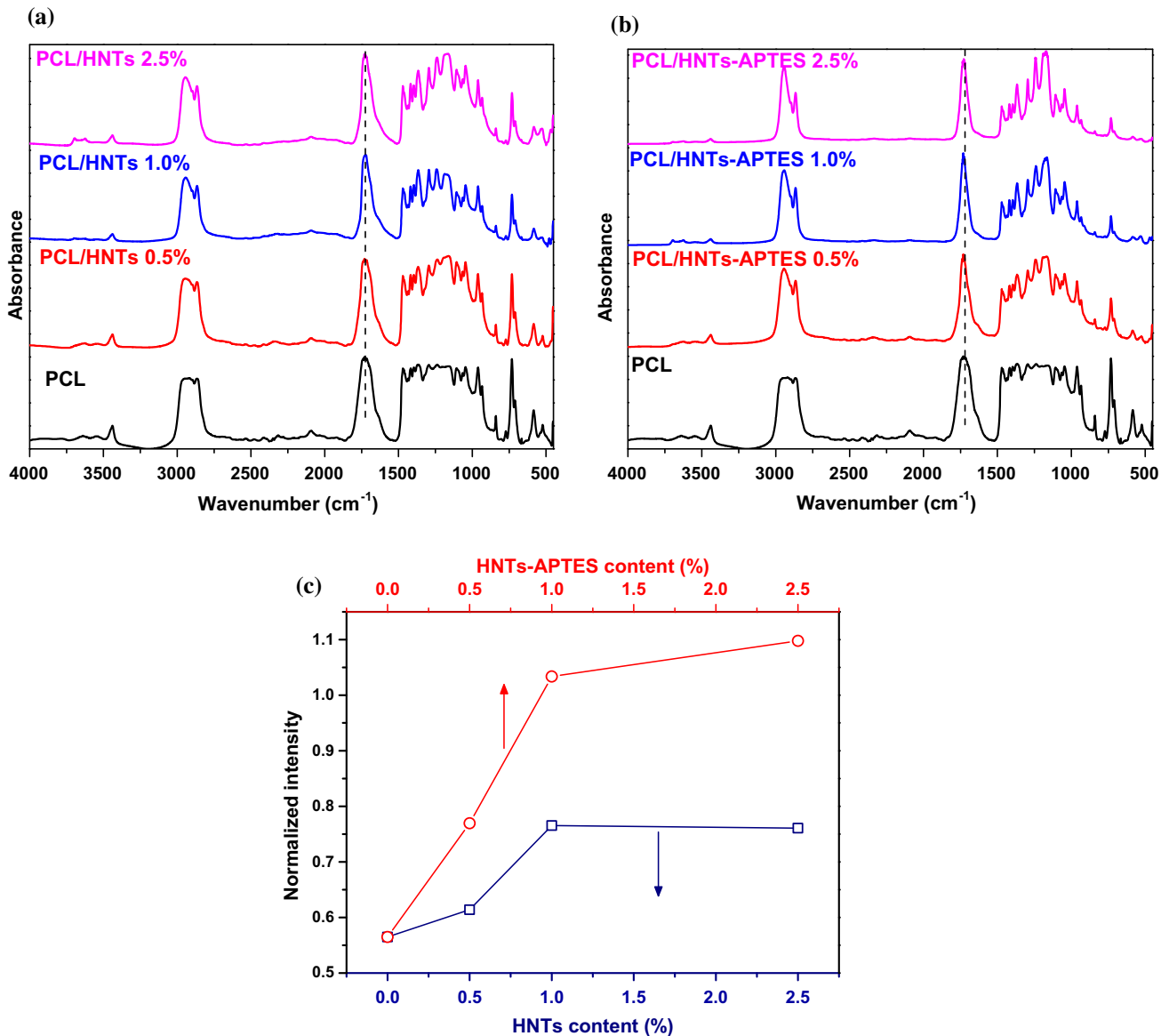


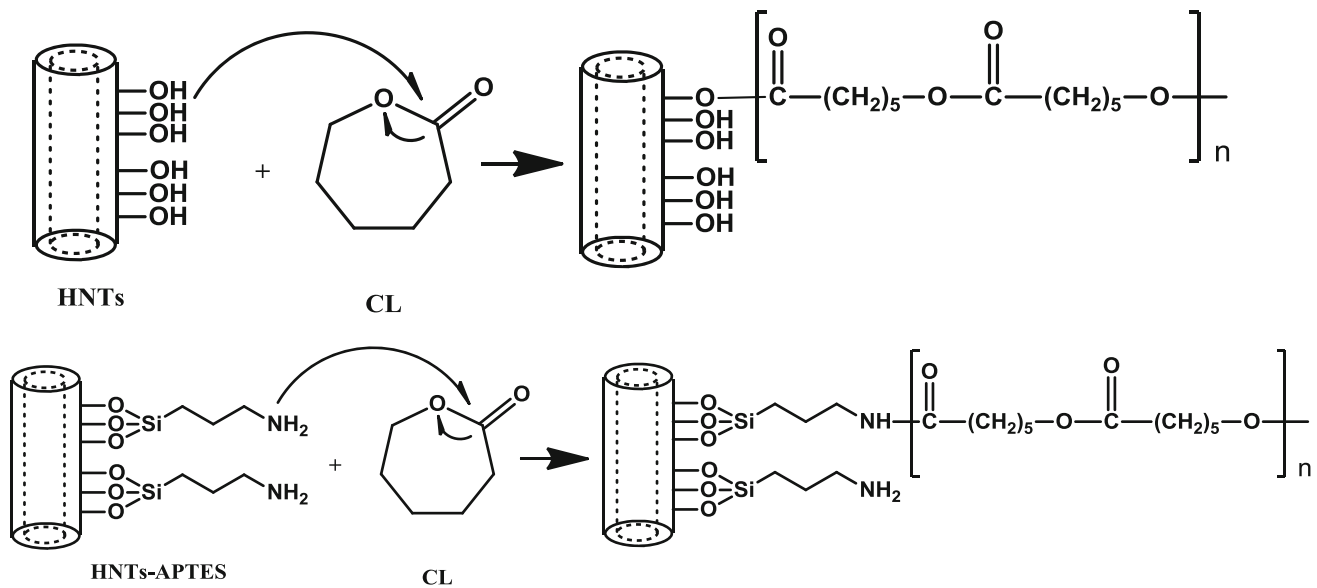
Figure 4 FTIR spectra of **a** PCL/HNTs, **b** PCL/HNTs–APTES and **c** carbonyl indices of PCL and its nanocomposites.

to the increased amount of carboxyl end groups, as the molecular weight decreases after the incorporation of nanofillers, while in the HNTs–APTES nanocomposites, the possible formation of amide bonds between the amino groups of the modified nanofiller and the carbonyl of the lactone may contribute in the increased amount of C=O groups. The possible resulting structure of the PCL/HNTs–APTES nanocomposites is presented in Scheme 2.

WAXD diffraction patterns of PCL and its nanocomposite are presented in Fig. 5, and the crystallinity values calculated by Eq. 1 in Table 4. PCL exhibits crystalline peaks at $2\theta = 21.54^\circ$, 22.12° and

23.8° that correspond to the (110), (111) and (200) planes of the orthorhombic unit cell [54]. Also, a small peak of PCL at about $2\theta = 17^\circ$ can be noticed [55–58], and its intensity is diminished in the presence of the nanofillers.

After the incorporation of the pristine and functionalized HNTs into PCL, the diffraction peaks did not shift, implying that the crystal structure of the polymeric matrix was not altered by the nanofillers. Additionally, the peaks of pure HNTs and HNTs–APTES did not appear in the patterns of the nanocomposites, which is an indication of good dispersion and absence of aggregates [59]. However, it is



Scheme 2 Schematic presentation of in situ synthesis of PCL/HNTs and PCL/HNTs-APTES nanocomposites.

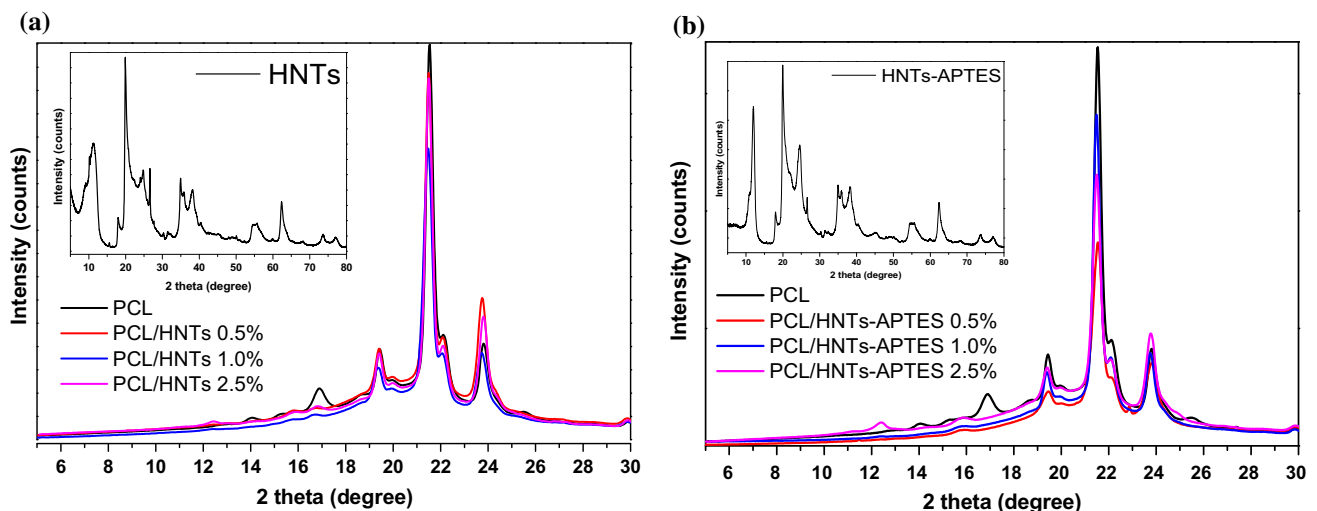


Figure 5 WAXD patterns of **a** PCL/HNTs nanocomposites and **b** PCL/HNTs-APTES nanocomposites (inset: X-ray diffractograms of the respective nanofillers).

Table 4 X_c (%) of the polyesters as calculated by WAXD

Sample	X_c (%)
PCL	45.88
PCL/HNTs 0.5%	47.05
PCL/HNTs 1.0%	47.19
PCL/HNTs 2.5%	50.03
PCL/HNTs-APTES 0.5%	55.44
PCL/HNTs-APTES 1.0%	45.38
PCL/HNTs-APTES 2.5%	47.94

also possible that the diffraction peaks of HNTs could not be detected due to the small amount of fillers in the polymer.

The WAXD profiles were fitted with Gaussian-Lorentzian cross product curves and the results are presented in Fig. S8. The crystallinity X_c % of the polymers was calculated by obtaining the ratio of the area of crystalline peaks over the overall area under the diffractogram, and the values are presented in Table 4. There are no major differences between the crystallinity of the matrix and the nanocomposites, as expected due to the small amount of filler.

Thermal characterization

The thermal properties of PCL and nanocomposites were evaluated by DSC. Like most nanofillers, HNTs can accelerate the crystallization behavior of PCL, which is generally a slow-crystallizing polyester, by acting as heterogeneous nucleation points [60, 61]. As it can be seen in Fig. S9, the glass transition temperature (T_g) of the matrix and the composites was observed at $-63\text{ }^\circ\text{C}$, while the melting temperature (T_m) was observed at $56\text{ }^\circ\text{C}$. The presence of the fillers did not seem to affect the thermal characteristics (T_g , T_m) of the matrix during the initial assessment. The crystallization behavior is very important aspect of their nature as it can determine their final degree of crystallinity and the morphology of the materials after processing [62]. Several studied have found that silicon-based nanofillers like Polyhedral Oligomeric Silsesquioxanes (POSS) enhance the isothermal melt crystallization of PCL in low concentrations [63–65], as well as carbon-based nanofillers [66]. In the following, we will evaluate the crystallization behavior of PCL and nanocomposites under isothermal and dynamic conditions.

Isothermal crystallization: Avrami theory The samples were crystallized at different temperatures, namely 40, 42, 44 and 46 $^\circ\text{C}$ and the heat flow curves with increasing time were obtained, as shown in Fig. S10 only for pure PCL, for brevity reasons. Moreover, the relative degree of crystallinity was obtained from Eq. 4:

$$X(t) = \frac{\int_0^t (dH_c/dt)dt}{\int_0^\infty (dH_c/dt)dt} \tag{4}$$

where dH_c denotes the measured enthalpy of crystallization during an infinitesimal time interval dt .

The evolution of the relative degree of crystallinity versus time can be seen in Fig. 6, for pure PCL and for the PCL/HNTs–APTES 1% sample, at different crystallization temperatures. It is obvious that the crystallization time increases with increasing temperature, indicating that nucleation is a limited parameter of crystallization, while the presence of the functionalized fillers in the nanocomposite sample enabled faster crystallization, as it was expected. The half-time of crystallization ($t_{1/2}$) was obtained from the curves in Fig. 6, and the results are presented in

Fig. 7. All nanocomposites exhibit smaller $t_{1/2}$ than the matrix, but it is also important to notice that the $t_{1/2}$ of the nanocomposites containing the functionalized filler accelerated the crystallization of PCL, as a result of the enhanced interactions with the matrix.

A number of macrokinetic models have been proposed in literature [62] to describe the effect of the fillers on isothermal crystallization, but the theory proposed by Avrami [67–69] is most probably the most used one. According to the modified Avrami method, the relative degree of crystallinity can be calculated from Eq. 5:

$$X(t) = 1 - \exp(-kt^n) \quad \text{or} \quad X(t) = 1 - \exp[-(Kt)^n] \tag{5}$$

where n is the Avrami exponent, a function of the nucleation process and k is the growth function, which is dependent on nucleation and crystal growth. Since the units of k are a function of n , the Avrami equation can be written in the composite Avrami form using $k = K^n$. In this work, the nonlinear curve fitting procedure was followed, based on the Levenberg–Marquardt method and the results are summarized in Table 5. The guidelines presented from Lorenzo et al. on the correct use of Avrami equation to fit the isothermal crystallization data, were carefully followed [70]. It can be seen that for all samples, n was between 2.5 and 4, indicating 3-dimensional nucleation [43]. Moreover, the growth function decreased with increasing T_c and increased with increasing filler content, consistent with the results from the $t_{1/2}$.

Lauritzen–Hoffman analysis The kinetic data from isothermal crystallization has also been analyzed with Lauritzen–Hoffman secondary nucleation theory [71]. According to this, the growth rate G is given as a function of temperature T_c by Eq. 6:

$$G = G_0 \exp\left[-\frac{U^*}{R(T_c - T_\infty)}\right] \exp\left[\frac{K_g}{T_c(\Delta T)f}\right] \tag{6}$$

where the first exponential term contains the contribution of the diffusion process to the growth rate and G_0 is the pre-exponential factor, while the second exponential term represents the contribution of the nucleation process. Moreover, the term U^* denoted the activation energy of the molecular diffusion across the interfacial boundary between crystalline

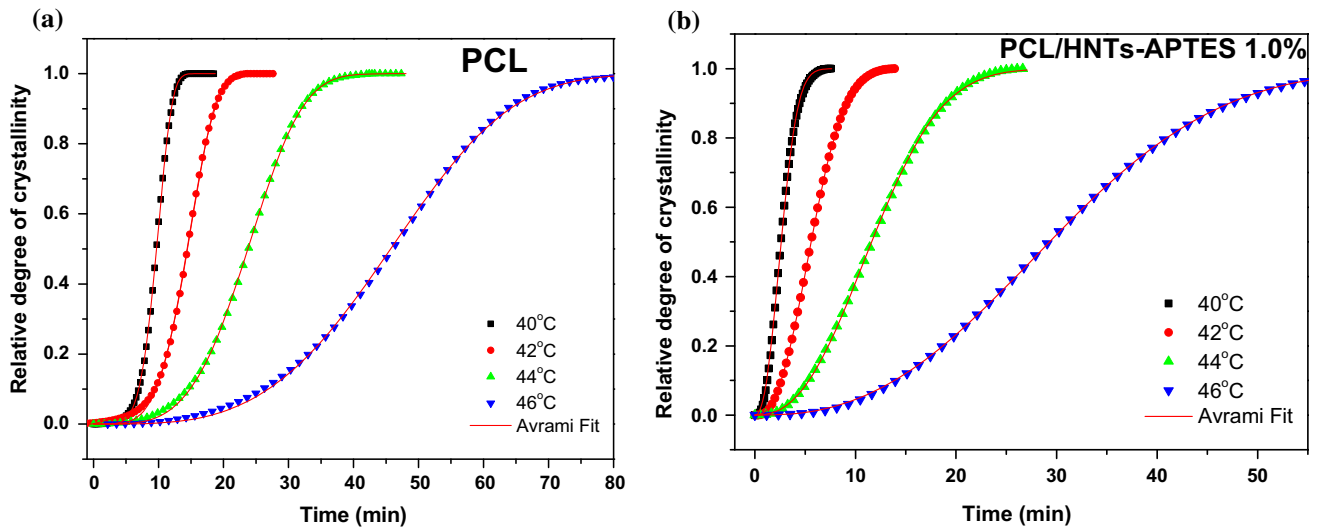


Figure 6 Evolution of relative degree of crystallinity as a function of time for **a** PCL and **b** PCL/HNT–APTES 1.0% under isothermal conditions.

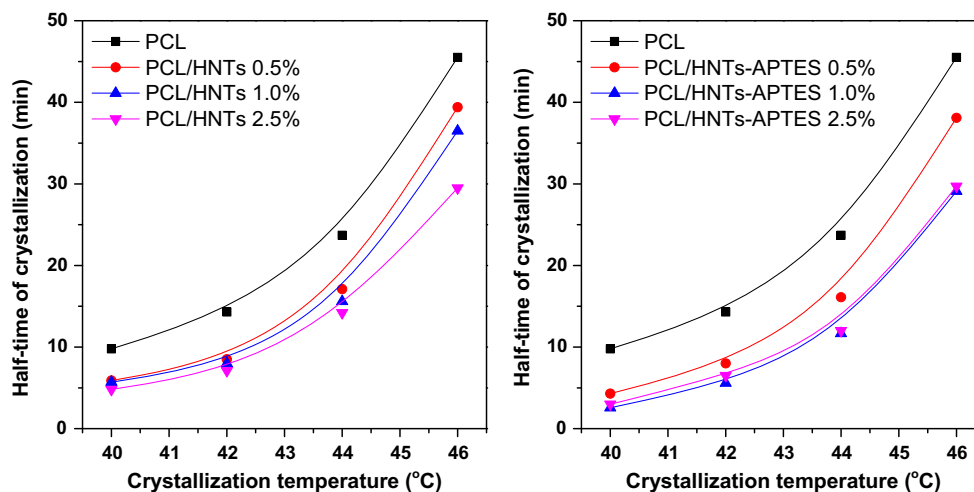


Figure 7 Half-time of crystallization versus the crystallization temperature for each sample.

and melt state and it is usually set at $1500 \text{ cal mol}^{-1}$. Also, $T_{\infty} = T_g - 30 \text{ K}$, and it is the temperature below which the diffusion stops, ΔT denotes the degree of undercooling ($\Delta T = T_m^0 - T_c$), f is a correction factor which is close to unity at high temperatures and is given as $f = 2T_c / (T_m^0 + T_c)$, while K_g is the nucleation parameter. In the current work, the equilibrium melting point was set equal to $78 \text{ }^{\circ}\text{C}$ for PCL, while the $T_g = -66 \text{ }^{\circ}\text{C}$. The nucleation parameter K_g can be obtained by the double logarithmic transformation of Eq. 7:

$$\ln(G) + \frac{U^*}{R(T_c - T_{\infty})} = \ln(G_0) - \frac{K_g}{T_c(\Delta T)f} \quad (7)$$

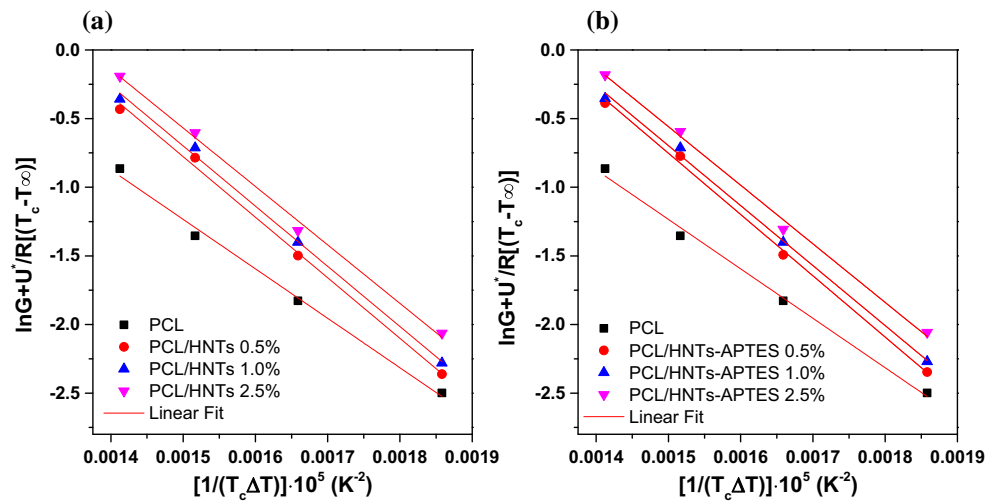
and after plotting the left-hand side of Eq. 7 with respect to $1/T_c(\Delta T)f$ a straight line should appear with a slope equal to K_g .

The common empirical approximation of the spherulite growth rate is inversely proportional to the crystallization half-time $G \approx 1/t_{1/2}$ has been used here for the evaluation of the nucleation parameter [72]. The $t_{1/2}$ values presented earlier have been used for this reason and the Lauritzen–Hoffman type plots for PCL and nanocomposites are presented in Fig. 8. In addition, for a secondary or heterogeneous nucleation, K_g can be obtained from Eq. 8:

Table 5 Avrami parameters of PCL and nanocomposites

Crystallization temperature (°C)	PCL		PCL/HNTs 0.5 wt%		PCL/HNTs 1.0 wt%		PCL/HNTs 2.5 wt%	
	<i>n</i>	<i>K</i> (min ⁻¹)	<i>n</i>	<i>K</i> (min ⁻¹)	<i>n</i>	<i>K</i> (min ⁻¹)	<i>n</i>	<i>K</i> (min ⁻¹)
40	2.6	0.8	3	0.94	2.9	1.22	3.2	1.39
42	2.8	0.4	3.1	0.74	3.4	0.99	3.3	1.16
44	2.9	0.1	3.2	0.45	3.5	0.84	3.6	0.93
46	3.1	0.06	3.6	0.33	4	0.52	3.8	0.76
			PCL/HNTs–APTES 0.5 wt%		PCL/HNTs–APTES 1 wt%		PCL/HNTs–APTES 2.5 wt%	
40			2.4	1.14	2.6	1.48	2.8	1.51
42			2.5	0.97	2.7	1.19	3	1.17
44			2.6	0.73	2.9	0.93	3.1	0.9
46			2.9	0.61	3.1	0.81	3.2	0.76

Figure 8 Lauritzen–Hoffman plots for **a** PCL/HNTs and **b** PCL/HNTs–APTES nanocomposites.



$$K_g = \frac{j b_0 \sigma \sigma_e T_m^0}{k_B (\Delta h_f)} \tag{8}$$

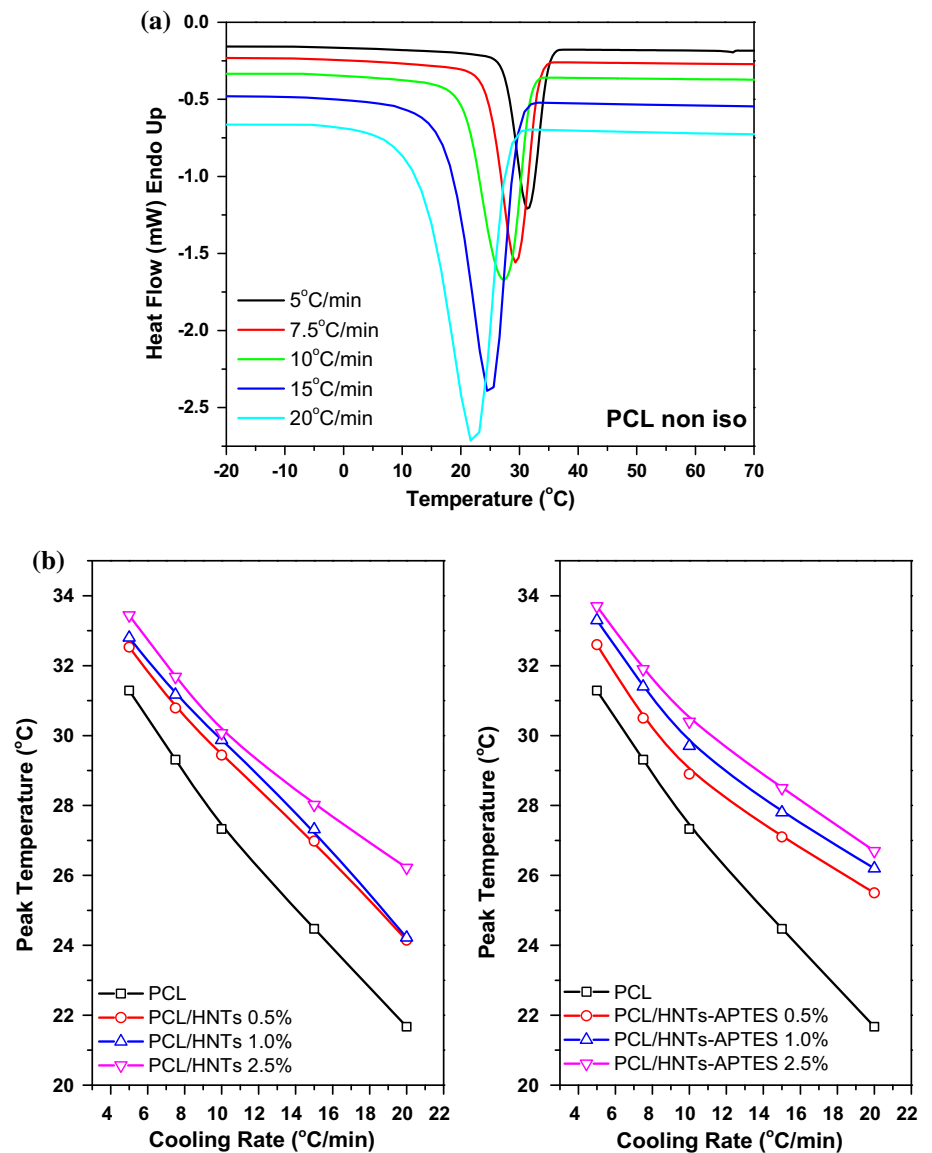
where *j* is a constant equal to 2 for regime II and equal to 4 for regime I and III, also σ , σ_e are the side surface (lateral) and fold surface (end) free energies which represent the work needed for the creation of a new surface, $\Delta h_f \rho_c = \Delta H_f$ is the enthalpy of melting per unit volume, b_0 is the single layer thickness, and k_B is the Boltzmann constant ($k_B = 1.38 \cdot 10^{-23} \text{ J K}^{-1}$). The values used here were $a_0 = 4.5 \text{ \AA}$, $b_0 = 4.1 \text{ \AA}$, and $U^* = 1500 \text{ cal mol}^{-1}$ which correspond to PCL and were also adopted for all materials. ΔH_f for PCL was taken equal to 136 J g^{-1} , while the unit cell density was taken 1.175 g cm^{-3} . Moreover, it was supposed that regime II holds at this temperature range and thus $j = 2$. According to Thomas and Staveley, the lateral surface free energy can be

obtained by $\sigma = \alpha \Delta h_f \sqrt{a_0 b_0}$ where the a_0 and b_0 factors are the molecular width and the molecular layer thickness, respectively, and α was derived to be empirically equal to 0.1 as this is a commonly accepted value for flexible polyesters [72]. Finally, the work of chain folding can be obtained from the fold surface free energy as $q = 2 \sigma_e \alpha_0 b_0$.

The calculated values of K_g can be found in Table 6, and it can be seen that they are lower than the ones of PCL for all nanocomposite samples. This is an indication that the foreign particles within PCL reduce the critical nucleus size needed for crystal growth and the free energy that acts against primary nucleation. Moreover, the lower values of the work of chain folding q for the nanocomposites indicate that the folding of macromolecular chains proceeds easier (especially in the samples filled with HNTs–APTES),

Table 6 Results from the Lauritzen–Hoffman analysis for PCL and nanocomposites

Material	K_{gII} ($\times 10^5$ K ²)	$\sigma\sigma_e$ ($\times 10^{-4}$ J ² /m ⁴)	σ (J ² /m ²)	σ_e (J ² /m ²)	q (kJ/mol)
PCL	0.89	7.56	68.8×10^{-4}	0.11	24.4
PCL–HNTs 0.5%	0.78	6.32	68.8×10^{-4}	0.092	20.4
PCL–HNTs 1.0%	0.75	6.12	68.8×10^{-4}	0.089	19.7
PCL–HNTs 2.5%	0.69	5.77	68.8×10^{-4}	0.084	18.6
PCL–HNTs–APTES 0.5%	0.71	5.71	68.8×10^{-4}	0.087	19.3
PCL–HNTs–APTES 1.0%	0.65	5.09	68.8×10^{-4}	0.074	16.4
PCL–HNTs–APTES 2.5%	0.63	4.81	68.8×10^{-4}	0.07	15.5

Figure 9 **a** DSC cooling curves of non-isothermal crystallization of PCL, **b** peak temperatures for non-isothermal crystallization of PCL and nanocomposites.

therefore facilitating the growth of crystals. The results are very close to previously published literature works [73, 74].

Non-isothermal Crystallization The dynamic crystallization of PCL from the melt in the presence of untreated and functionalized HNTs was studied in

detail. Figure 9a shows the characteristic DSC scans for the crystallization of PCL in a range of cooling rates (5–20 °C min⁻¹). As expected, the crystallization peaks moved to lower temperatures with increasing cooling rate, while the variation of the peaks for PCL and nanocomposites is presented in Fig. 9b. It can be seen that the differences are quite small and the crystallization of the nanocomposites took place 2–3 °C higher than the matrix. Moreover, the functionalized nanofillers crystallized at slightly higher temperatures than their unfunctionalized counterparts as a result of enhanced interactions with the matrix and optimum dispersion, which are known to affect the crystallization procedure. The nucleating effect of nanofillers on PCL has been observed by several research groups [74–78].

Nucleation Activity The nucleation activity of the HNTs within the PCL was calculated with the theory proposed by Dobрева and Gutzow [79, 80]. In this method, the nucleation activity (ϕ) is a factor which describes the work of three-dimensional nucleation and it decreases with the addition of a filler particle within the matrix. If the filler is extremely active, then $\phi \approx 0$, while if it is inert then $\phi \approx 1$. The nucleation activity is calculated by the ratio:

$$\phi = \frac{B^*}{B} \tag{9}$$

where the parameter B can be obtained from the slope of Eq. 10, after plotting $\ln(\beta)$ versus the inverse squared degree of supercooling $1/\Delta T_p^2$ ($\Delta T_p = T_m - T_p$):

$$\ln \beta = \text{Const} - \frac{B}{\Delta T_p^2} \tag{10}$$

For the case of heterogeneous nucleated by using a nucleating agent, Eq. 10 is transformed to the following:

$$\ln \beta = \text{Const} - \frac{B^*}{\Delta T_p^2} \tag{11}$$

The plots of $\ln \beta$ versus $1/\Delta T_p^2$ can be seen in Fig. 10a for all the nanocomposites under study. Straight lines were obtained for every samples, while from the slope of the linear fits the values of B and B^* can be calculated. Then, the nucleation activity can be obtained from the B^*/B ratio and the results are presented in Fig. 10b. As it was described earlier, the

lower the B^*/B ratio, the higher the nucleation activity, while values close to 1 indicate low nucleation activity. It is obvious from Fig. 10b that the unfunctionalized HNTs do not affect heavily the crystallization of PCL, being almost inert during the crystallization process ($\phi \approx 0.95$). On the other hand, the functionalized HNTs display higher nucleation activity with the sample filled with 1 wt% HNTs–APTES being more active, probably as a result of optimum dispersion and stronger interactions.

Effective activation energy The calculation of the effective activation energy can provide insights on the crystallization behavior of polymer nanocomposites [81]. A number of models have been proposed in literature, but the most used one is the one proposed by Kissinger [81]:

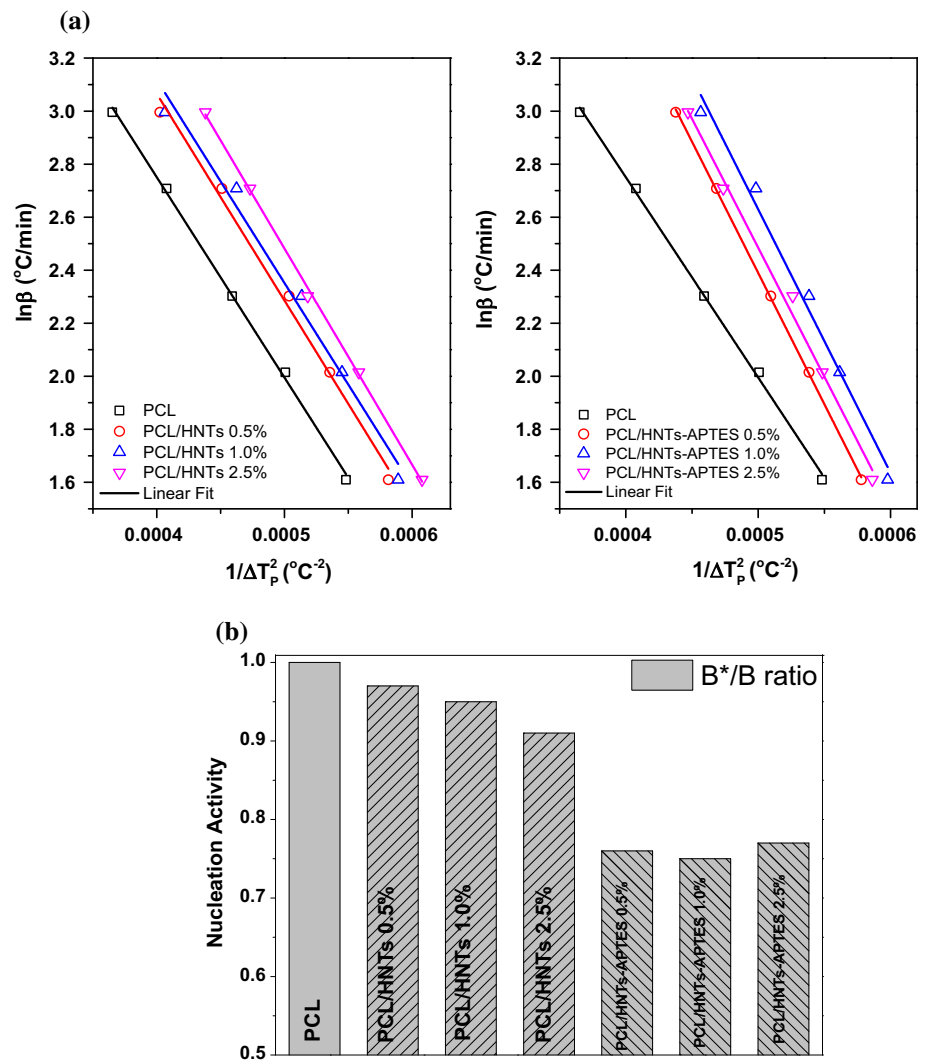
$$\ln\left(\frac{\beta}{T_p^2}\right) = \text{Const.} - \frac{\Delta E}{RT_p} \tag{12}$$

where β is the cooling rate, T_p is the peak temperature and R is the universal gas constant. Vyazovkin and Sbirrazzuoli have shown that the negative values of the logarithm of the cooling rate β , which is present in the Kissinger equation, represent a mathematically invalid procedure; therefore, this theory cannot be used in non-isothermal crystallization from the melt [81]. Another issue of the method is that it assumes that the processes described are modeled using single-step kinetics; however, polymer crystallization is a quite complex procedure; thus, the use of multiple heating/cooling rates is recommended [82]. An isoconversional method is therefore suggested for the calculation of the effective activation energy during non-isothermal crystallization. The differential isoconversional method of Friedman [83] and the advanced integral method of Sbirrazzuoli and Vyazovkin [84] are the most popular ones and in this work, the method of Friedman was applied to the data from the dynamic crystallization of the nanocomposites. In this method, the activation energy takes different values for different degrees of crystallinity:

$$\ln\left(\frac{dX}{dt}\right)_{X,i} = \text{Const.} - \frac{\Delta E_X}{RT_{X,i}} \tag{13}$$

where dX/dt is the instantaneous crystallization rate as a function of time at a given conversion X , ΔE_X is

Figure 10 a Dobrev plots for PCL and nanocomposites, b calculated nucleation activity of the nanocomposites.



the effective activation energy at a given degree of conversion, $T_{X,i}$ is the set of temperatures related to a given conversion X at different cooling rates and the i subscript refers to different cooling rates that were used during the experimental procedure. The instantaneous crystallization rate is obtained by differentiating the $X(t)$ function obtained from the integration of the experimentally measured crystallization, with respect to time. Furthermore, the values of dX/dt at a specific X are correlated to the corresponding crystallization temperature at this X (i.e., T_X), by selecting appropriate degrees of crystallinity (i.e., from 5 to 95%). Then, by plotting the left-hand side of Eq. 13 with respect to $1/T_X$, a straight line must be obtained with a slope equal to $\Delta E_X/R$.

The results from the calculation of E for PCL and nanocomposites can be seen in Fig. 11. It should be noted that the negative E values for PCL and

nanocomposites indicate that the crystallization of polymers is a spontaneous process and that the rate of crystallization increased with decreasing temperature [84] and this observation has been confirmed for several thermoplastics in the literature [5, 6, 47, 85–87]. For neat PCL, the activation energy is higher than that of the nanocomposites, while it can be seen that E keeps increasing with increasing degree of crystallinity, indicating that the phenomenon is more demanding energetically at higher X_c . Interestingly, the curves of the activation energy between the two sets of fillers display some differences between them. The activation energy of the nanocomposites with the functionalized filler present a sudden drop at around 50% crystallinity and from $X_c \approx 60\%$ they start to increase again, while the E values do not change significantly with increasing filler content. It should be stated that the effective

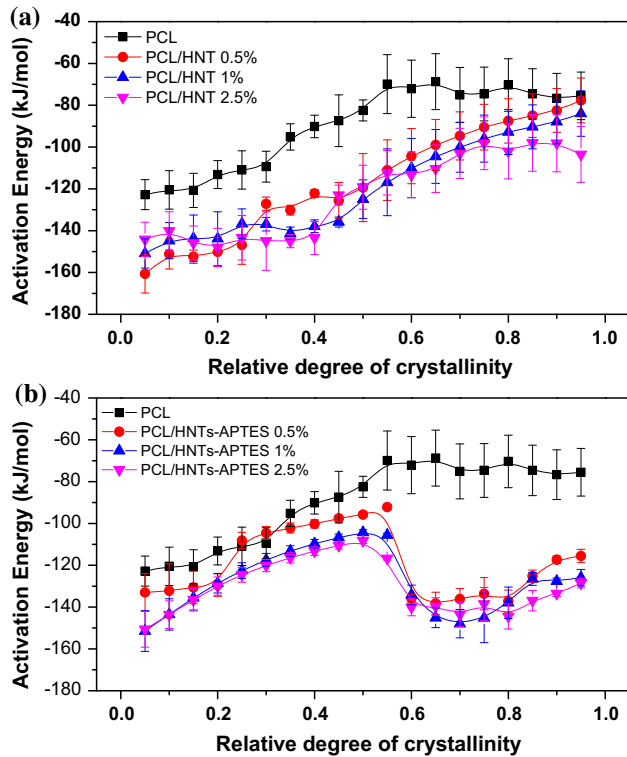


Figure 11 Effective activation energy as a function of relative degree of crystallinity for **a** PCL/HNT and **b** PCL/HNTs–APTES samples.

activation energy here has the meaning of the temperature coefficient of the crystallization rate [88]. This dependence of E on X_c for the PCL/HNTs–APTES samples is an indication of a complex crystallization mechanism, different than the neat polymer and the unfunctionalized nanocomposites.

Polarizing light microscopy Polarized light optical microscopy was utilized in order to observe the spherulitic morphology of PCL and nanocomposites during isothermal crystallization. From the images presented in Table 7, it can be seen that the nucleation density of the nanocomposite samples is much higher than the matrix, as a result of the fillers acting as heterogeneous nucleating agents during crystallization. Moreover, the size of the spherulites decreases significantly after the introduction of the functionalized filler, as a result of enhanced crystallization rates and homogeneous distribution of the filler.

Thermogravimetric analysis Thermal stability of the nanocomposites was studied by TGA, with the resulting curves presented in Fig. 12, and the characteristic temperatures of degradation presented in Table 8, as well as the % inorganic content at 600 °C. HNTs did not affect the thermal stability of PCL, and

Table 7 Spherulites of PCL and its nanocomposites grown at 42, 46 and 48 °C (magnification 40×)

	42 °C (15 min)	46 °C (30 min)	48 °C (45 min)
PCL			
PCL/HNTs 2.5 wt%			
PCL/HNTs–APTES 2.5 wt%			

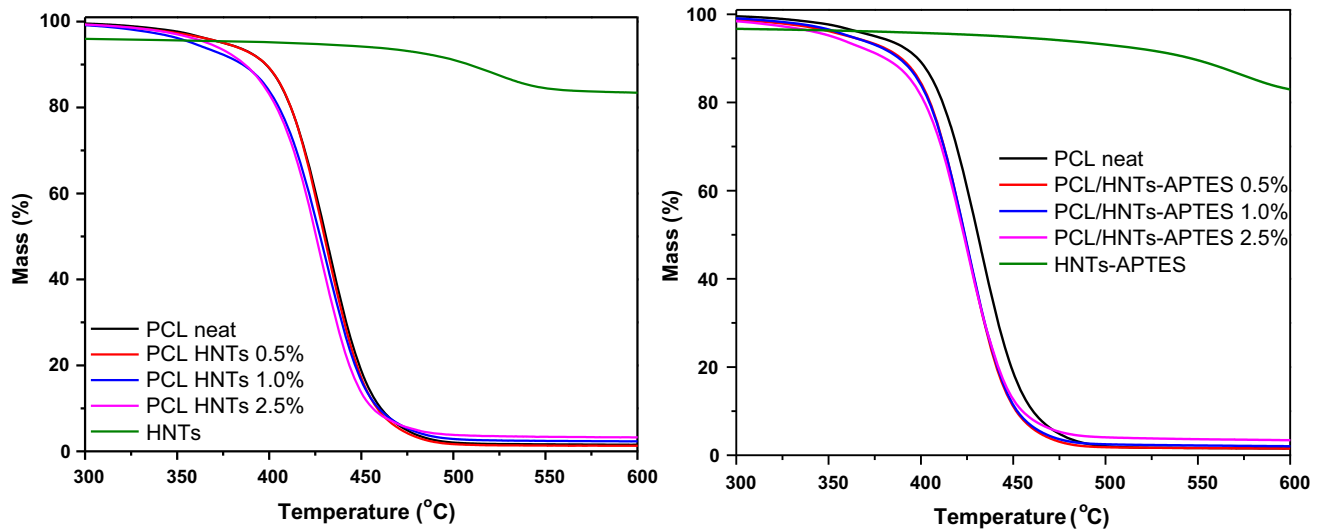


Figure 12 TGA curves of PCL and its nanocomposites with HNTs and HNTs–APTES.

Table 8 Characteristic temperatures of thermal degradation and residue of PCL and its nanocomposites

Sample	$T_{d,2\%wt}$ (°C)	T_{max} (°C)	Residue at 600 °C (%)
PCL	345.1	431.7	1.28
PCL HNTs 0.5%	338.3	429.6	1.54
PCL HNTs 1%	327.5	430.4	2.32
PCL HNTs 2.5%	336.9	427.4	3.24
PCL HNTs APTES 0.5%	322.9	425.6	1.52
PCL HNTs APTES 1%	330.6	425.3	2.42
PCL HNTs APTES 2.5%	310.6	424.7	3.42

the recorded T_{max} values were ranging from 427 to 431 °C, with insignificant variations. The free hydroxyls on the inner surface of HNTs and the subsequent moisture they can entrap prevent the otherwise thermally stable nanotubes from decelerating the thermal decomposition of PCL [60]. In the presence of HNTs–APTES, a small decrease in T_{max} was observed, of about 5 °C for all filler contents. Organosilane-modified nanofillers cannot improve the thermal stability of polymers, probably due to the thermally unstable organic functional group of the silane. Functionalized clay minerals can catalyze polymer degradation due to the presence of Lewis acidic sites on their edges after the degradation of the modification agent [89, 90]. Additionally, the free amino groups of HNTs–APTES can cause aminolytic decomposition of PCL [91]. In all cases, degradation occurs in a single step, between 300 and 450 °C, suggesting no changes in the decomposition mechanism were caused by the presence of the nanofillers. Regarding the mass residue at 600 °C, the inorganic

content of the nanocomposites was very close to the initial amounts of nanofillers used. The thermal stability of PCL can be either enhanced or reduced by HNTs. When increase in thermal stability was reported, it was attributed to the inherent excellent thermal stability of the nanotubes, and their action as mass and heat transport barriers [92, 93]. Decrease in thermal stability has also been reported, and was caused by the presence of water molecules inside the lumens of HNTs [94].

Conclusions

Nanocomposites of PCL with HNTs and functionalized HNTs–APTES were successfully synthesized with the in situ ring-opening polymerization method. Both nanofillers were found able to act as co-initiators, as evidenced by the decrease in the IV and \bar{M}_n values of the nanocomposites. SEM micrographs indicated good dispersion of the fillers since there

were no visible aggregates. The presence of the nanofillers enhanced slightly the crystallization rates of the matrix, with the functionalized nanotubes being more effective toward the nucleation of PCL, as a result of homogeneous dispersion and stronger interfacial interactions. From Lauritzen–Hoffman analysis, it was found that the fillers reduced the critical nucleus size needed for crystal growth and the free energy that acts against primary nucleation, while the folding of the macromolecular chains proceeds easier in the case of the PCL/HNTs–APTES samples. The thermal stability of PCL was not reduced by HNTs, but by HNTs–APTES which were found capable of catalyzing the polymer's degradation. Solid residues values at 600 °C were very close to the initial amount of nanofillers added.

Acknowledgements

The authors would like to thank Associate Professor Konstantinos Triantafyllidis of the Laboratory of Chemical and Environmental Technology, Department of Chemistry, Aristotle University of Thessaloniki, for the nitrogen adsorption/desorption experiments.

Compliance with ethical standards

Conflict of interest The authors declare no conflict of interest.

Electronic supplementary material: The online version of this article (<https://doi.org/10.1007/s10853-018-1993-1>) contains supplementary material, which is available to authorized users.

References

- [1] Liu M, Jia Z, Jia D, Zhou C (2014) Recent advance in research on halloysite nanotubes-polymer nanocomposite. *Prog Polym Sci* 39:1498–1525. <https://doi.org/10.1016/j.progpolymsci.2014.04.004>
- [2] Bhattacharya M (2016) Polymer nanocomposites-A comparison between carbon nanotubes, graphene, and clay as nanofillers. *Materials (Basel)* 9:1–35. <https://doi.org/10.3390/ma9040262>
- [3] Bikiaris D (2011) Can nanoparticles really enhance thermal stability of polymers? Part II: an overview on thermal decomposition of polycondensation polymers. *Thermochim Acta* 523:25–45. <https://doi.org/10.1016/j.tca.2011.06.012>
- [4] Chrissafis K, Bikiaris D (2011) Can nanoparticles really enhance thermal stability of polymers? Part I: an overview on thermal decomposition of addition polymers. *Thermochim Acta* 523:1–24. <https://doi.org/10.1016/j.tca.2011.06.010>
- [5] Papageorgiou GZ, Achilias DS, Bikiaris DN, Karayannidis GP (2005) Crystallization kinetics and nucleation activity of filler in polypropylene/surface-treated SiO₂ nanocomposites. *Thermochim Acta* 427:117–128. <https://doi.org/10.1016/j.tca.2004.09.001>
- [6] Papageorgiou GZ, Karandrea E, Giliopoulos D et al (2014) Effect of clay structure and type of organomodifier on the thermal properties of poly(ethylene terephthalate) based nanocomposites. *Thermochim Acta* 576:84–96. <https://doi.org/10.1016/j.tca.2013.12.006>
- [7] Papageorgiou GZ, Terzopoulou Z, Achilias DS et al (2013) Biodegradable poly(ethylene succinate) nanocomposites. Effect of filler type on thermal behaviour and crystallization kinetics. *Polymer (United Kingdom)* 54:4604–4616. <https://doi.org/10.1016/j.polymer.2013.06.005>
- [8] Papageorgiou GZ, Terzopoulou Z, Bikiaris D et al (2014) Evaluation of the formed interface in biodegradable poly(l-lactic acid)/graphene oxide nanocomposites and the effect of nanofillers on mechanical and thermal properties. *Thermochim Acta* 597:48–57. <https://doi.org/10.1016/j.tca.2014.10.007>
- [9] Terzopoulou Z, Patsiaoura D, Papageorgiou DG et al (2017) Effect of MWCNTs and their modification on crystallization and thermal degradation of poly(butylene naphthalate). *Thermochim Acta* 656:59–69. <https://doi.org/10.1016/j.tca.2017.08.012>
- [10] Sengupta R, Bhattacharya M, Bandyopadhyay S, Bhowmick AK (2011) A review on the mechanical and electrical properties of graphite and modified graphite reinforced polymer composites. *Prog Polym Sci* 36:638–670
- [11] Leslie-Pelecky DL, Rieke RD (1996) Magnetic properties of nanostructured materials. *Chem Mater* 8:1770–1783. <https://doi.org/10.1021/cm960077f>
- [12] Sanchez C, Lebeau B, Chaput F, Boilot J-P (2003) Optical properties of functional hybrid organic-inorganic nanocomposites. *Adv Mater* 15:1969–1994. <https://doi.org/10.1002/adma.200300389>
- [13] Armentano I, Dottori M, Fortunati E et al (2010) Biodegradable polymer matrix nanocomposites for tissue engineering: a review. *Polym Degrad Stab* 95:2126–2146. <https://doi.org/10.1016/j.polymdegradstab.2010.06.007>

- [14] Klopogge JT (1998) Synthesis of smectites and porous pillared clay catalysts: a review. *J Porous Mater* 5:5–41. <https://doi.org/10.1023/A:1009625913781>
- [15] Murray HH (1991) Overview—clay mineral applications. *Appl Clay Sci* 5:379–395. [https://doi.org/10.1016/0169-1317\(91\)90014-Z](https://doi.org/10.1016/0169-1317(91)90014-Z)
- [16] Joussein E, Petit S, Churchman J et al (2005) Halloysite clay minerals—a review. *Clay Miner* 40:383–426. <https://doi.org/10.1180/0009855054040180>
- [17] Lvov YM, DeVilliers MM, Fakhrullin RF (2016) The application of halloysite tubule nanoclay in drug delivery. *Expert Opin Drug Deliv* 5247:1–10. <https://doi.org/10.1517/17425247.2016.1169271>
- [18] Du M, Guo B, Jia D (2010) Newly emerging applications of halloysite nanotubes: a review. *Polym Int* 59:574–582. <https://doi.org/10.1002/pi.2754>
- [19] Peixoto AF, Fernandes AC, Pereira C et al (2016) Physicochemical characterization of organosilylated halloysite clay nanotubes. *Microporous Mesoporous Mater* 219:145–154. <https://doi.org/10.1016/j.micromeso.2015.08.002>
- [20] Labet M, Thielemans W (2009) Synthesis of polycaprolactone: a review. *Chem Soc Rev* 38:3484. <https://doi.org/10.1039/b820162p>
- [21] Mondal D, Griffith M, Venkatraman SS (2016) Polycaprolactone-based biomaterials for tissue engineering and drug delivery: current scenario and challenges. *Int J Polym Mater Polym Biomater* 65:255–265. <https://doi.org/10.1080/00914037.2015.1103241>
- [22] Marco Zanetti, Sergei L, Giovanni Camino (2000) Polymer layered silicate nanocomposites. *Macromol Mater Eng* 279:1–9. [https://doi.org/10.1002/1439-2054\(20000601\)279:1%3C1::AID-MAME1%3E3.0.CO;2-Q/full](https://doi.org/10.1002/1439-2054(20000601)279:1%3C1::AID-MAME1%3E3.0.CO;2-Q/full)
- [23] Kuo SW, Huang WJ, Huang SB et al (2003) Syntheses and characterizations of in situ blended metalocene polyethylene/clay nanocomposites. *Polymer (Guildf)* 44:7709–7719. <https://doi.org/10.1016/j.polymer.2003.10.007>
- [24] Kim J, Kwak S, Hong SM et al (2010) Nonisothermal crystallization behaviors of nanocomposites prepared by in situ polymerization of high-density polyethylene on multiwalled carbon nanotubes. *Macromolecules* 43:10545–10553. <https://doi.org/10.1021/ma102036h>
- [25] Zou H, Wu S, Shen J (2008) Polymer/silica nanocomposites: preparation, characterization, properties, and applications. *Chem Rev* 108:3893–3957. <https://doi.org/10.1021/cr068035q>
- [26] Vikas M (ed) (2011) In-situ synthesis of polymer nanocomposites. In: *In-situ synthesis of polymer nanocomposites*. Wiley, Weinheim, pp 1–25
- [27] Lahcini M, Elhakioui S, Szopinski D et al (2016) Harnessing synergies in tin-clay catalyst for the preparation of poly(ϵ -caprolactone)/halloysite nanocomposites. *Eur Polym J* 81:1–11. <https://doi.org/10.1016/j.eurpolymj.2016.05.014>
- [28] Bhagabati P, Chaki TK, Khastgir D (2015) One-step in situ modification of halloysite nanotubes: augmentation in polymer-filler interface adhesion in nanocomposites. *Ind Eng Chem Res* 54:6698–6712. <https://doi.org/10.1021/acs.iecr.5b01043>
- [29] Vieira Marques MDF, da Silva Rosa JL, da Silva MCV (2017) Nanocomposites of polypropylene with halloysite nanotubes employing in situ polymerization. *Polym Bull* 74:2447–2464. <https://doi.org/10.1007/s00289-016-1848-3>
- [30] Zhao M, Liu P (2008) Halloysite nanotubes/polystyrene (HNTs/PS) nanocomposites via in situ bulk polymerization. *J Therm Anal Calorim* 94:103–107. <https://doi.org/10.1007/s10973-007-8677-4>
- [31] Lin Y, Ng KM, Chan C-M et al (2011) High-impact polystyrene/halloysite nanocomposites prepared by emulsion polymerization using sodium dodecyl sulfate as surfactant. *J Colloid Interface Sci* 358:423–429. <https://doi.org/10.1016/j.jcis.2011.03.009>
- [32] Barkoula NM, Alcock B, Cabrera NO, Peijs T (2008) Fatigue properties of highly oriented polypropylene tapes and all-polypropylene composites. *Polym Polym Compos* 16:101–113
- [33] Marini J, Pollet E, Averous L, Bretas RES (2014) Elaboration and properties of novel biobased nanocomposites with halloysite nanotubes and thermoplastic polyurethane from dimerized fatty acids. *Polymer (Guildf)* 55:5226–5234. <https://doi.org/10.1016/j.polymer.2014.08.049>
- [34] Gong B, Ouyang C, Gao Q et al (2016) Synthesis and properties of a millable polyurethane nanocomposite based on castor oil and halloysite nanotubes. *RSC Adv* 6:12084–12092. <https://doi.org/10.1039/C5RA21586B>
- [35] Haroosh HJ, Dong Y, Chaudhary DS et al (2013) Electrospun PLA: pCL composites embedded with unmodified and 3-aminopropyltriethoxysilane (ASP) modified halloysite nanotubes (HNT). *Appl Phys A Mater Sci Process* 110:433–442. <https://doi.org/10.1007/s00339-012-7233-7>
- [36] Du M, Guo B, Liu M, Jia D (2006) Preparation and characterization of polypropylene grafted halloysite and their compatibility effect to polypropylene/halloysite composite. *Polym J* 38:1198–1204. <https://doi.org/10.1295/polymj.PJ2006038>
- [37] Albdiry MT, Yousif BF (2013) Morphological structures and tribological performance of unsaturated polyester based untreated/silane-treated halloysite nanotubes. *Mater Des* 48:68–76. <https://doi.org/10.1016/j.matdes.2012.08.035>

- [38] Chen S, Lu X, Wang T, Zhang Z (2015) Preparation and characterization of mechanically and thermally enhanced polyimide/reactive halloysite nanotubes nanocomposites. *J Polym Res*. <https://doi.org/10.1007/s10965-015-0806-3>
- [39] Roumeli E, Papageorgiou DG, Tsanaktsis V et al (2015) Amino-functionalized multiwalled carbon nanotubes lead to successful ring-opening polymerization of poly(ϵ -caprolactone): enhanced interfacial bonding and optimized mechanical properties. *ACS Appl Mater Interfaces* 7:11683–11694. <https://doi.org/10.1021/acsami.5b03693>
- [40] Shi Y-F, Tian Z, Zhang Y et al (2011) Functionalized halloysite nanotube-based carrier for intracellular delivery of antisense oligonucleotides. *Nanoscale Res Lett* 6:608. <https://doi.org/10.1186/1556-276X-6-608>
- [41] Roumeli E, Avgeropoulos A, Pavlidou E et al (2014) Understanding the mechanical and thermal property reinforcement of crosslinked polyethylene by nanodiamonds and carbon nanotubes. *RSC Adv* 4:45522–45534. <https://doi.org/10.1039/c4ra05585c>
- [42] Roumeli E, Pavlidou E, Avgeropoulos A et al (2014) Factors controlling the enhanced mechanical and thermal properties of nanodiamond-reinforced cross-linked high density polyethylene. *J Phys Chem B*. <https://doi.org/10.1021/jp504531f>
- [43] Vassiliou AA, Papageorgiou GZ, Achilias DS, Bikiaris DN (2007) Non-isothermal crystallisation kinetics of in situ prepared poly(ϵ -caprolactone)/surface-treated SiO₂ nanocomposites. *Macromol Chem Phys* 208:364–376. <https://doi.org/10.1002/macp.200600447>
- [44] Michell RM, Mugica A, Zubitur M, Müller AJ (2017) Self-nucleation of crystalline phases within homopolymers, polymer blends, copolymers, and nanocomposites. In: Auriemma F, Alfonso GC, de Rosa C (eds) *Polymer crystallization I: from chain microstructure to processing*. Springer, Cham, pp 215–256
- [45] Arnal ML, Balsamo V, Ronca G et al (2000) Applications of successive self-nucleation and annealing (SSA) to polymer characterization. *J Therm Anal Calorim* 59:451–470. <https://doi.org/10.1023/A:1010137408023>
- [46] Muller AJ, Albuerno J, Marquez L et al (2005) Self-nucleation and crystallization kinetics of double crystalline poly(p-dioxanone)-b-poly(ϵ -caprolactone) diblock copolymers. *Faraday Discuss* 128:231–252. <https://doi.org/10.1039/B403085K>
- [47] Yuan P, Southon PD, Liu Z et al (2008) Functionalization of halloysite clay nanotubes by grafting with γ -aminopropyltriethoxysilane. *J Phys Chem C* 112:15742–15751. <https://doi.org/10.1021/jp805657t>
- [48] Ng KM, Lau YTR, Chan CM et al (2011) Surface studies of halloysite nanotubes by XPS and ToF-SIMS. *Surf Interface Anal* 43:795–802. <https://doi.org/10.1002/sia.3627>
- [49] Hillier S, Brydson RIK, Delbos E et al (2016) Correlations among the mineralogical and physical properties of halloysite nanotubes (HNTs). *Clay Miner* 51:1–59
- [50] Hu P, Yang H (2013) Insight into the physicochemical aspects of kaolins with different morphologies. *Appl Clay Sci* 74:58–65. <https://doi.org/10.1016/j.clay.2012.10.003>
- [51] Luo P, Zhang J, Zhang B et al (2011) Preparation and characterization of silane coupling agent modified halloysite for Cr(VI) removal. *Ind Eng Chem Res* 50:10246–10252
- [52] Kricheldorf HR, Berl M, Scharnagl N (1988) Poly(lactones). 9. Polymerization Mechanism of metal alkoxide initiated polymerizations of lactide and various lactones. *Macromolecules* 21:286–293
- [53] Papageorgiou DG, Kinloch IA, Young RJ (2017) Mechanical properties of graphene and graphene-based nanocomposites. *Prog Mater Sci* 90:75–127
- [54] Navarro-Baena I, Marcos-Fernandez A, Kenny JM, Peponi L (2014) Crystallization behavior of diblock copolymers based on PCL and PLLA biopolymers. *J Appl Crystallogr* 47:1948–1957. <https://doi.org/10.1107/S1600576714022468>
- [55] Abdelrazek EM, Hezma AM, El-khodary A, Elzayat AM (2016) Spectroscopic studies and thermal properties of PCL/PMMA biopolymer blend. *Egypt J Basic Appl Sci* 3:10–15. <https://doi.org/10.1016/j.ejbas.2015.06.001>
- [56] Gloria A, Russo T, D'Amora U et al (2013) Magnetic poly(ϵ -caprolactone)/iron-doped hydroxyapatite nanocomposite substrates for advanced bone tissue engineering. *J R Soc Interface* 10:20120833. <https://doi.org/10.1098/rsif.2012.0833>
- [57] Rezaei A, Mohammadi MR (2013) In vitro study of hydroxyapatite/polycaprolactone (HA/PCL) nanocomposite synthesized by an in situ sol-gel process. *Mater Sci Eng C* 33:390–396. <https://doi.org/10.1016/j.msec.2012.09.004>
- [58] Fabbri P, Bondioli F, Messori M et al (2010) Porous scaffolds of polycaprolactone reinforced with in situ generated hydroxyapatite for bone tissue engineering. *J Mater Sci Mater Med* 21:343–351. <https://doi.org/10.1007/s10856-009-3839-5>
- [59] Roop S, Das A, Thakur V et al (2010) Preparation and properties of natural nanocomposites based on natural rubber and naturally occurring halloysite nanotubes. *Mater Des* 31:2151–2156. <https://doi.org/10.1016/j.matdes.2009.11.009>
- [60] Tham WL, Poh BT, Mohd Ishak ZA, Chow WS (2014) Thermal behaviors and mechanical properties of halloysite nanotube-reinforced poly(lactic acid) nanocomposites. *J Therm Anal Calorim* 118:1639–1647. <https://doi.org/10.1007/s10973-014-4062-2>

- [61] Lee K-S, Chang Y-W (2013) Thermal, mechanical, and rheological properties of poly(ϵ -caprolactone)/halloysite nanotube nanocomposites. *J Appl Polym Sci* 128:2807–2816. <https://doi.org/10.1002/app.38457>
- [62] Di Lorenzo ML, Silvestre C (1999) Non-isothermal crystallization of polymers. *Prog Polym Sci* 24:917–950. [https://doi.org/10.1016/S0079-6700\(99\)00019-2](https://doi.org/10.1016/S0079-6700(99)00019-2)
- [63] Nerantzaki M, Papageorgiou GZ, Bikiaris DN (2014) Effect of nanofiller's type on the thermal properties and enzymatic degradation of poly(ϵ -caprolactone). *Polym Degrad Stab* 108:257–268. <https://doi.org/10.1016/j.polymdegradstab.2014.03.018>
- [64] Guan W, Qiu Z (2012) Isothermal crystallization kinetics, morphology, and dynamic mechanical properties of biodegradable poly(ϵ -caprolactone) and octavinyl-polyhedral oligomeric silsesquioxanes nanocomposites. *Ind Eng Chem Res* 51:3203–3208. <https://doi.org/10.1021/ie202802d>
- [65] Pan H, Yu J, Qiu Z (2011) Crystallization and morphology studies of biodegradable poly(ϵ -caprolactone)/polyhedral oligomeric silsesquioxanes nanocomposites. *Polym Eng Sci* 51:2159–2165. <https://doi.org/10.1002/pen.21983>
- [66] Qiu Z, Wang H, Xu C (2011) Crystallization, mechanical properties, and controlled enzymatic degradation of biodegradable poly(ϵ -caprolactone)/multi-walled carbon nanotubes nanocomposites. *J Nanosci Nanotechnol* 11:7884–7893. <https://doi.org/10.1166/jnn.2011.4714>
- [67] Avrami M (1941) Granulation, phase change, and microstructure kinetics of phase change III. *J Chem Phys* 9:177–184. <https://doi.org/10.1063/1.1750872>
- [68] Avrami M (1940) Kinetics of phase change. II transformation-time relations for random distribution of nuclei. *J Chem Phys* 8:212–224. <https://doi.org/10.1063/1.1750631>
- [69] Avrami M (1939) Kinetics of phase change. I general theory. *J Chem Phys* 7:1103–1112. <https://doi.org/10.1063/1.1750380>
- [70] Lorenzo AT, Arnal ML, Albuerne J, Müller AJ (2007) DSC isothermal polymer crystallization kinetics measurements and the use of the Avrami equation to fit the data: guidelines to avoid common problems. *Polym Test* 26:222–231. <https://doi.org/10.1016/j.polymertesting.2006.10.005>
- [71] Hoffman JD, Miller RL (1997) Kinetic of crystallization from the melt and chain folding in polyethylene fractions revisited: theory and experiment. *Polymer (Guildf)* 38:3151–3212. [https://doi.org/10.1016/S0032-3861\(97\)00071-2](https://doi.org/10.1016/S0032-3861(97)00071-2)
- [72] Papageorgiou DG, Papageorgiou GZ, Bikiaris DN, Christafis K (2013) Crystallization and melting of propylene-ethylene random copolymers. Homogeneous nucleation and β -nucleating agents. *Eur Polym J* 49:1577–1590. <https://doi.org/10.1016/j.eurpolymj.2013.02.002>
- [73] Nanaki SG, Papageorgiou GZ, Bikiaris DN (2012) Crystallization of novel poly(ϵ -caprolactone)-block-poly(propylene adipate) copolymers. *J Therm Anal Calorim* 108:633–645. <https://doi.org/10.1007/s10973-011-2155-8>
- [74] Lopez JV, Perez-Camargo RA, Zhang B et al (2016) The influence of small amounts of linear polycaprolactone chains on the crystallization of cyclic analogue molecules. *RSC Adv* 6:48049–48063. <https://doi.org/10.1039/C6RA04823D>
- [75] Di Maio E, Iannace S, Sorrentino L, Nicolais L (2004) Isothermal crystallization in PCL/clay nanocomposites investigated with thermal and rheometric methods. *Polymer (Guildf)* 45:8893–8900. <https://doi.org/10.1016/j.polymer.2004.10.037>
- [76] Siqueira G, Fraschini C, Bras J et al (2011) Impact of the nature and shape of cellulosic nanoparticles on the isothermal crystallization kinetics of poly(ϵ -caprolactone). *Eur Polym J* 47:2216–2227. <https://doi.org/10.1016/j.eurpolymj.2011.09.014>
- [77] Zhuravlev E, Schmelzer JWP, Wunderlich B, Schick C (2011) Kinetics of nucleation and crystallization in poly(ϵ -caprolactone) (PCL). *Polymer (Guildf)* 52:1983–1997. <https://doi.org/10.1016/j.polymer.2011.03.013>
- [78] Di Y, Iannace S, Di Maio E, Nicolais L (2003) Nanocomposites by melt intercalation based on polycaprolactone and organoclay. *J Polym Sci Part B Polym Phys* 41:670–678. <https://doi.org/10.1002/polb.10420>
- [79] Dobreva A, Gutzow I (1993) Activity of substrates in the catalyzed nucleation of glass-forming melts. I. Theory. *J Non Cryst Solids* 162:1–12. [https://doi.org/10.1016/0022-3093\(93\)90736-H](https://doi.org/10.1016/0022-3093(93)90736-H)
- [80] Dobreva A, Gutzow I (1993) Activity of substrates in the catalyzed nucleation of glass-forming melts. II. Experimental evidence. *J Non Cryst Solids* 162:13–25. [https://doi.org/10.1016/0022-3093\(93\)90737-I](https://doi.org/10.1016/0022-3093(93)90737-I)
- [81] Vyazovkin S, Dranca I (2006) Isoconversional analysis of combined melt and glass crystallization data. *Macromol Chem Phys* 207:20–25. <https://doi.org/10.1002/macp.200500419>
- [82] Vyazovkin S, Burnham AK, Criado JM et al (2011) ICTAC kinetics committee recommendations for performing kinetic computations on thermal analysis data. *Thermochim Acta* 520:1–19. <https://doi.org/10.1016/j.tca.2011.03.034>
- [83] Friedman HL (1964) Kinetics of thermal degradation of char-forming plastics from thermogravimetry. Application to a phenolic plastic. *J Polym Sci Part C Polym Symp* 6:183–195. <https://doi.org/10.1002/polc.5070060121>
- [84] Vyazovkin S, Sbirrazzuoli N (2002) Isoconversional analysis of the nonisothermal crystallization of a polymer melt. *Macromol Rapid Commun* 23:766–770. <https://doi.org/10.1002/mrca.10022>

- 1002/1521-3927(20020901)23:13<766::AID-MARC766>3.0.CO;2-0/abstract
- [85] Bosq N, Guigo N, Zhuravlev E, Sbirrazzuoli N (2013) Nonisothermal crystallization of polytetrafluoroethylene in a wide range of cooling rates. *J Phys Chem B* 117:3407–3415. <https://doi.org/10.1021/jp311196g>
- [86] Vyazovkin S, Sbirrazzuoli N (2003) Estimating the activation energy for non-isothermal crystallization of polymer melts. *J Therm Anal Calorim* 72:681–686. <https://doi.org/10.1023/A:1024506522878>
- [87] Papageorgiou DG, Chrissafis K, Pavlidou E et al (2014) Effect of nanofiller's size and shape on the solid state microstructure and thermal properties of poly(butylene succinate) nanocomposites. *Thermochim Acta* 590:181–190. <https://doi.org/10.1016/j.tca.2014.06.030>
- [88] Vyazovkin S, Sbirrazzuoli N (2004) Isoconversional approach to evaluating the Hoffman–Lauritzen parameters (U^* and K_g) from the overall rates of nonisothermal crystallization. *Macromol Rapid Commun* 25:733–738. <https://doi.org/10.1002/marc.200300295>
- [89] Dong Y, Marshall J, Haroosh HJ et al (2015) Polylactic acid (PLA)/halloysite nanotube (HNT) composite mats: influence of HNT content and modification. *Compos Part A Appl Sci Manuf* 76:28–36. <https://doi.org/10.1016/j.compositesa.2015.05.011>
- [90] Cervantes-Uc JM, Cauich-Rodríguez JV, Vázquez-Torres H et al (2007) Thermal degradation of commercially available organoclays studied by TGA–FTIR. *Thermochim Acta* 457:92–102. <https://doi.org/10.1016/j.tca.2007.03.008>
- [91] Papageorgiou DG, Roumeli E, Terzopoulou Z et al (2015) Polycaprolactone/multi-wall carbon nanotube nanocomposites prepared by in situ ring opening polymerization: decomposition profiling using thermogravimetric analysis and analytical pyrolysis-gas chromatography/mass spectrometry. *J Anal Appl Pyrolysis*. <https://doi.org/10.1016/j.jaap.2015.07.007>
- [92] Nitya G, Nair GT, Mony U et al (2012) In vitro evaluation of electrospun PCL/nanoclay composite scaffold for bone tissue engineering. *J Mater Sci Mater Med* 23:1749–1761. <https://doi.org/10.1007/s10856-012-4647-x>
- [93] Torres E, Fombuena V, Vallés-Lluch A, Ellingham T (2017) Improvement of mechanical and biological properties of polycaprolactone loaded with hydroxyapatite and halloysite nanotubes. *Mater Sci Eng C* 75:418–424. <https://doi.org/10.1016/j.msec.2017.02.087>
- [94] Jing X, Mi HY, Turng LS (2017) Comparison between PCL/hydroxyapatite (HA) and PCL/halloysite nanotube (HNT) composite scaffolds prepared by co-extrusion and gas foaming. *Mater Sci Eng C* 72:53–61. <https://doi.org/10.1016/j.msec.2016.11.049>